An Illustrated Overview of the Use and Value of a Wavelet Transformation to Acoustic Emission Technology

By

M.A. Hamstad

University of Denver, Denver, CO USA

National Institute for Science and Technology

Boulder, CO USA

This brief overview discusses a wavelet transformation (WT) relative to far-field acoustic emission (AE) signals in a plate-like test sample. Out-of-plane displacement signals in a plate are governed by the symmetric and anti-symmetric Lamb modes that are typically shown in the group velocity versus frequency•thickness curves. For a specific plate thickness, the displacement-signal energy is not uniformly distributed across the modes or along a single mode (as a function of frequency). Thus, the value of group-velocity curves by themselves is somewhat limited for the AE practitioner. However, a WT of an AE signal can communicate very useful information because it shows which modes carry significant energy and where (as a function of frequency) the significant energy is present within a mode. Figure 1 illustrates these aspects by displaying an AE signal and its WT with relevant curves from the group-velocity diagram superimposed. Note that the group-velocity axis has been changed to a time axis by use of the propagation distance of the AE signal. Clearly the WT contour plot of figure 1 shows that most of the AE signal energy (e.g., red areas) is located in two main areas: (a) the vicinity of 510 kHz with a group velocity of 1.8 mm/μs (based on the 180 mm propagation distance), and (b) the region of 65 to 75 kHz at velocities from 2.2 to 2.6 mm/μs. The wideband AE signal for this illustration was calculated by a finite element modeling (FEM) technique, but it could also be obtained experimentally from a truly wideband sensor.

From the point of view of application, the information in figure 1 could be used to select a resonant sensor and bandpass to enhance the signal-to-noise ratio at a known propagation velocity.

Figure 2 compares the WTs for AE signals (from FEM modeling) from an in-plane dipole and from the initiation of a microcrack. Clearly there are distinct differences in the frequency versus time information. Such differences show the potential for WTs to provide key information for AE source identification. Figure 3 shows the WTs from two AE signals from the same source type (an in-plane dipole) located at two different depths below the top surface of the plate. As the figure shows, the same source at different depths generates AE signals, which carry their significant energy in two different modes in two different frequency windows. Hence, further research needs to be done to deal with this depth dependence.

The time domain signal files which were used to generate the WTs in the figures above are included with the AGU-Vallen Wavelet software in *.tra format. The Wavelet program allows the standard time and frequency domains for the signals to be displayed as well as the WTs. The Wavelet program also allows the user to superimpose the relevant group-velocity curves (calculated with the included Dispersion program for the proper material and plate thickness and modified by the propagation distance) on the WT contour plot. All the files of the FEM generated signals (at a propagation distance of 180 mm) are from an aluminum sample of 4.7 mm thickness with sufficient transverse dimensions such that plate edge reflections are not present. The relevant bulk velocities used in the FEM simulation are 6320 m/s and 3100 m/s.

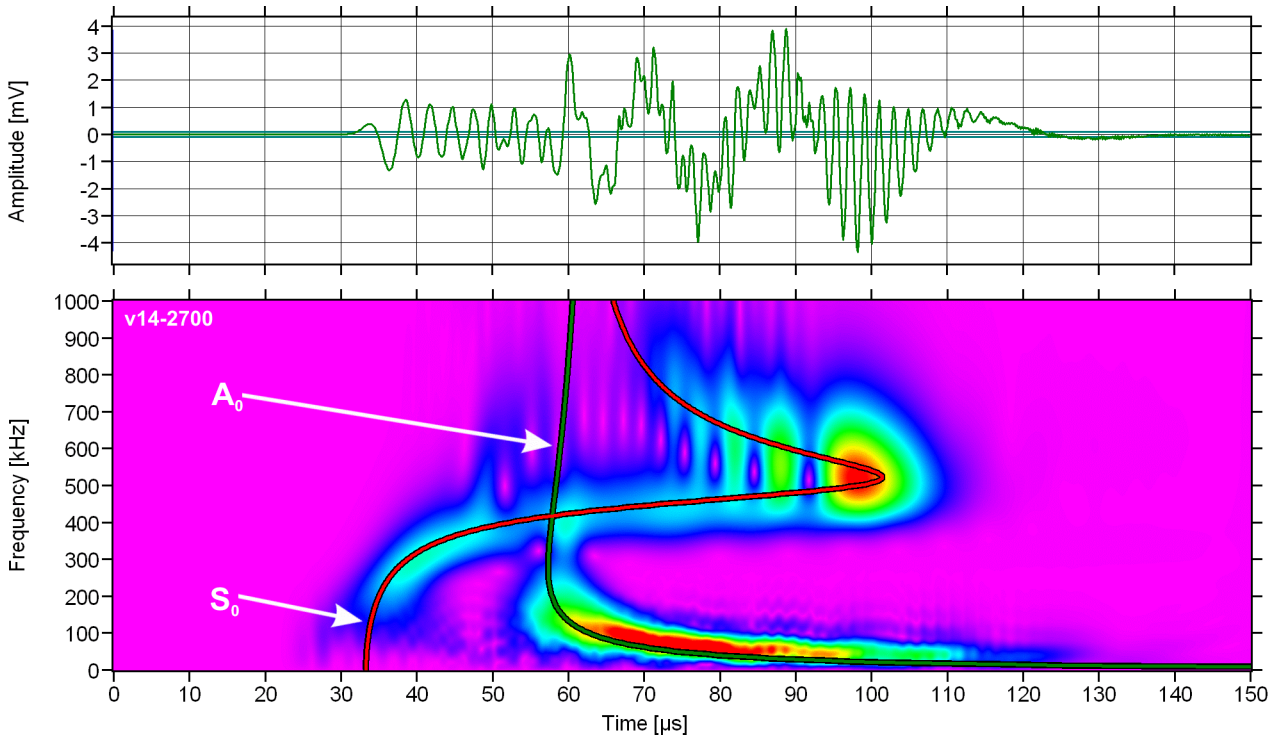

Figure 1: AE signal and its wavelet transform (multicolor area, red strongest) with superimposed modified group-velocity curves (fundamental modes, solid lines)

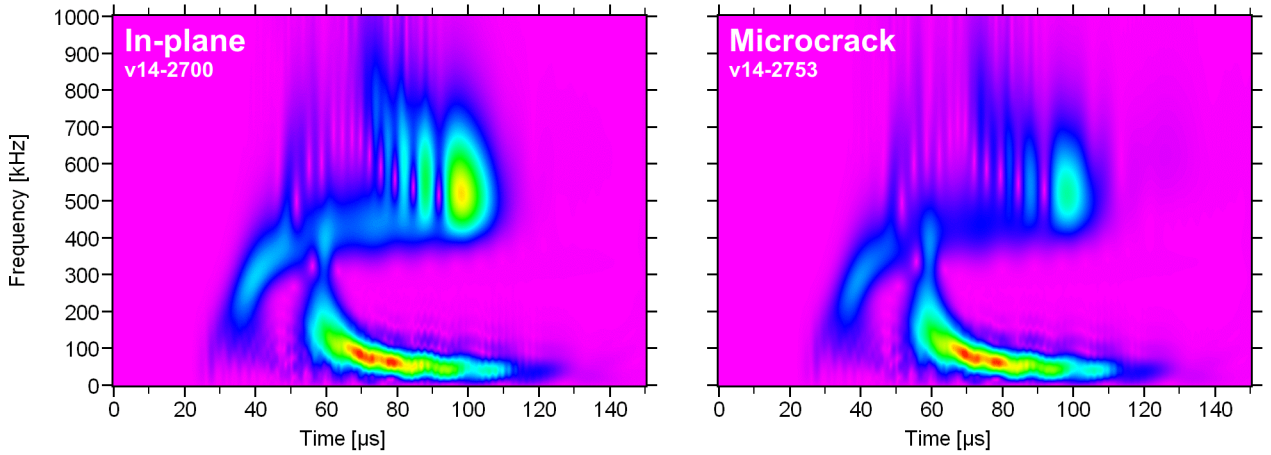

Figure 2: WTs of different AE sources; in-plane source (left) and microcrack initiation source (right)

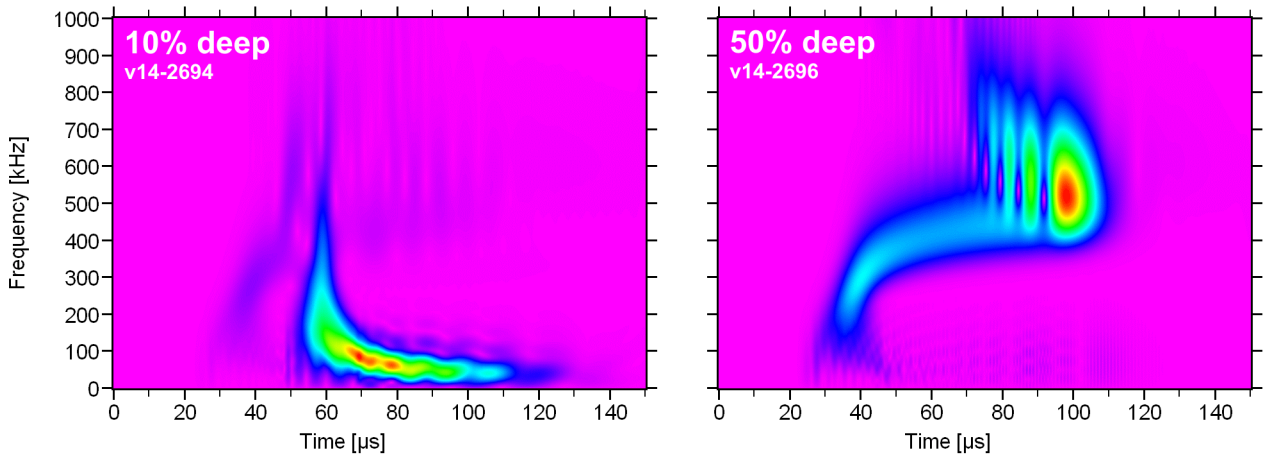

Figure 3: WTs of identical in-plane dipoles at two different depths below the top surface of the plate

A WAVELET TRANSFORM APPLIED TO ACOUSTIC EMISSION SIGNALS: PART 1: SOURCE IDENTIFICATION [#]

M. A. HAMSTAD[+], A. O'GALLAGHER and J. GARY

National Institute of Standards and Technology, Materials Reliability Division (853), Boulder, CO 80305-3328;
[+]Also Department of Engineering, University of Denver, Denver, CO 80208.

Abstract

A database of wideband acoustic emission (AE) modeled signals was used in Part 1 to examine the application of a wavelet transform (WT) to identify AE sources. The AE signals in the database were created by use of a validated three-dimensional finite element code. These signals represented the out-of-plane displacements from buried dipole sources in aluminum plates 4.7 mm thick and of small and large lateral dimensions. The surface displacement signals at three far-field distances were filtered with a 40 kHz high-pass filter prior to applying the WT. The WTs were calculated with AGU-Vallen Wavelet, a freeware software program. The effects of propagation distance, AE source type, and the depth of the AE source below the plate surface were examined. Specifically, a ratio of the WT magnitude (WT coefficient) from the fundamental anti-symmetric mode to that from the fundamental symmetric mode was studied for correlation with the AE source type. The WT magnitudes were those corresponding to a particular group velocity and signal frequency for each mode. For sources in the large plate located at the same depth, the ratios were able to distinguish different source types and exhibited only small changes with increasing propagation distance. But, when the variable of depth of the source was introduced, the ratios did not uniquely classify the AE source type. In the case of the small coupon plate specimen, reflections from the specimen edges distorted and complicated the WTs. Since the current coupon database excludes (except for one case) the parameter of changes in the distance of the source from the coupon sides, a full examination of these complications was not possible.

1. Introduction

Since early in the history of AE, a goal of AE practitioners has been to use AE signals as the means to identify the type of source that generated the signals (Mehan and Mullin, 1971). Papers have been published indicating the successful identification of AE sources, and commercial AE companies offer software for the purpose of identifying AE sources. These efforts are often controversial because they lack an analytical justification (based on the theory of AE) of the signal features used to sort the experimental signals into different types of sources. Alternatively, some AE source-identification experiments have been carried out with specimen geometries and sensor locations such that signals are obtained from the direct longitudinal bulk waves in several directions of radiation (Buttle and Scruby, 1990a). The analysis that is used to sort these signals into different source types (or combinations of source types) is based on analytical calculations (forward modeling) that determine the relative amplitudes of the first bulk longitudinal signals in different radiation directions. By comparing relative experimental bulk wave amplitudes in different directions with the calculated results for a series of possible sources, the experimental

sources were identified in a more satisfying fashion. However, in many AE applications Lamb waves are present due to plate-like test specimens and observation of the AE signals in the far-field. In this case, this more satisfying approach is not directly applicable. Some AE researchers (Weaver and Pao, 1982a, b; Guo et al., 1998) have presented analytical results (forward modeling) for Lamb waves in infinite plates, but to date they have not published an extensive database that could lead to source identification of experimental signals by appropriate comparisons.

The AE source-identification research presented here uses an extensive database of modeled Lamb-wave AE signals. These signals were obtained by use of a validated finite-element modeling code (Hamstad et al., 1999). Since the exact source type and all its characteristics are known for each signal, the features of the AE signals can be unequivocally associated with particular source types. In the case of experimental signals, this is not the case. In this paper we examine the possibilities of extracting meaningful source identification features by the use of a wavelet transform (WT). To retain the possibility of a direct method of source identification (rather that an artificial-intelligence method), this paper examines the extraction of limited data sets from the WT results. In addition, if the direct method is not completely successful, these results could provide insight into the most relevant WT results to input into an artificial-intelligence approach.

2. Description of AE Database

The AE signals that comprised the analyzed database were all calculated by the NIST- Boulder finite-element modeling (FEM) code. This code has been validated (Hamstad et al., 1999; Prosser et al., 1999) for buried dipole-type point sources operating in plate specimens with infinite lateral dimensions and for surface and edge monopole sources on plates with small and large lateral dimensions. The specimen domains in the database were aluminum plates 4.7 mm thick. These plates had lateral dimensions of either 1000 mm by 1000 mm (representing the infinite-plate case) or 480 mm by 25.4 mm (representing a small coupon specimen). Figure 1 shows a drawing of the small specimen superimposed on the large specimen. The lateral position of the AE source and the positions where the plate top surface out-of-plane displacement was determined as a function of time are shown. These displacement signals provide the AE signals that would be obtained in a single direction of radiation (toward sensors 1, 2 and 3) or the opposite direction (toward sensors 5, 6, and 7). All the sensor positions were 60 mm apart.

The calculated signals provided a unique and ideal database that was far superior to experimental AE signals for the study of AE source identification. The reasons for this superiority are due to exact knowledge of key information not always available in experimental data: point-source location in three dimensions; source rise time; magnitude and orientation of source dipoles; absolute out-of-plane displacement of a perfect wideband point sensor at an exact location; known filtering of the AE signal; signals both with specimen edge reflections and without such reflections; and signals that are largely free of noise.

For this study of AE source identification, the analyzed database included three types of buried point-sources: (1) in-plane dipole, aligned with the propagation direction to the sensors, (2) out-of-plane dipole, and (3) crack initiation (three dipoles) with the largest dipole aligned with the propagation direction to the sensors. The dipole forces (body forces) were all 1 N except for the two smaller dipoles in the microcrack case, which were 0.52 N (based on the elastic constants of aluminum). Each dipole was made up of a “central” cell having no body force, along with single cells on each side of the “central” cell having body forces. All the

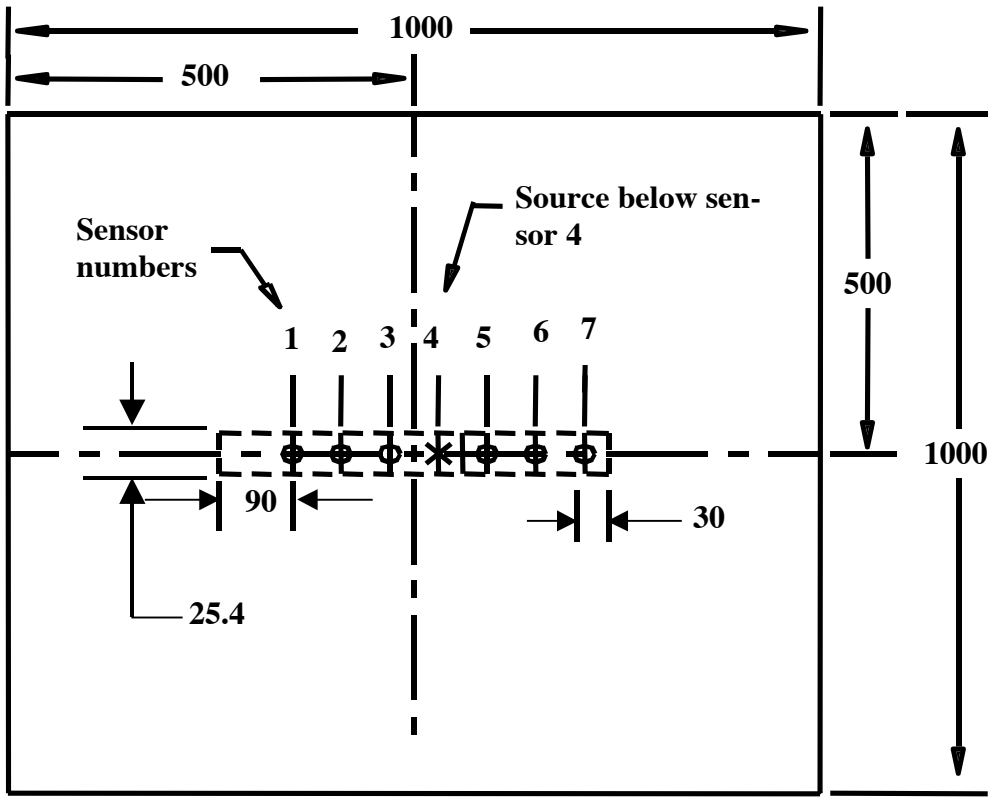

Fig. 1 Large specimen with superimposed small coupon specimen. Sensor positions, spaced 60 mm apart, show points where out-of-plane displacement was determined versus time. All dimensions in mm.

calculations were based on a uniform three-dimensional cell size of 0.313 mm, which was chosen to conform to the requirements for convergence (Hamstad et al., 1999). For the examination of propagation distance, the database included three propagation distances (60, 120, and 180 mm). The three distances were all in the far-field for the 4.7 mm thick plate. In addition, the database included the very important (as will be seen below) variable of depth of the point source below the top surface of the plate. All the sources had a rise time (of the dipole) of 1.5 μs with a "cosine bell" temporal dependence (Hamstad et al., 1999). This rise time resulted in AE signals with frequencies up to about 1 MHz (as determined from spectra calculated by a Fast Fourier Transform (FFT)). To provide a realistic database, all the AE signals were filtered with a 40 kHz high-pass four-pole Butterworth filter prior to analysis. Also, to represent experimental practice, all the calculated digital signals were resampled to a time step of 0.1 μs from the original calculation time step of 0.045 μs. Comparisons demonstrated that this resampling had no apparent effect on the waveforms or their FFTs. The calculated total signal length in each case was 200 μs beginning from the start of operation of the AE source.

3. General Examination of WT Results

Figure 2 shows an example of an AE signal without edge reflections and its calculated WT magnitude (WT coefficients) as a function of frequency versus time. The source for this signal was an in-plane dipole centered at a depth of 1.723 mm (the center of the "central" cell) below the plate top surface. The signal represents the top-surface out-of-plane displacement at 180 mm from the epicenter of the source. All the WTs were calculated with AGU-Vallen Wavelet, a freeware software program (Vallen-Systeme GmbH, 2001; H. Suzuki et al., 1996). AGU-Vallen

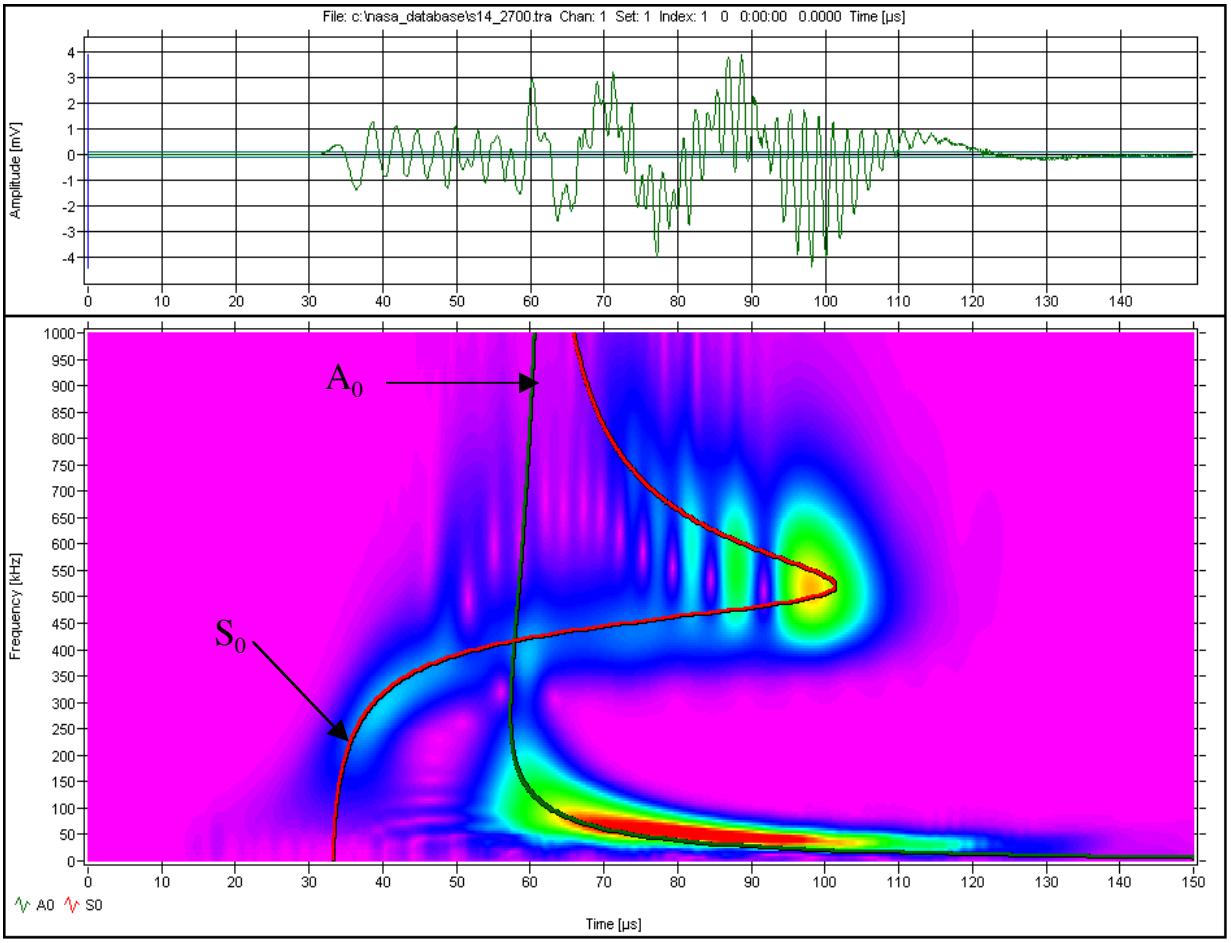

Fig. 2 Typical calculated AE signal from an in-plane dipole source with corresponding WT. Superimposed fundamental symmetric, So, and anti-symmetric, Ao, modes after converting group velocity to time based on 180 mm propagation distance. Red color corresponds to highest magnitude of the WT. Source depth is 1.723 mm in large specimen. (WT scale: 1 MHz: 150 µs)

Wavelet has been developed in collaboration between Vallen-Systeme GmbH and Aoyama Gakuin University (AGU), Tokyo, Japan. The AGU group has pioneered in the research of wavelet analysis in the field of acoustic emission (Suzuki et al., 1996; Takemoto et al., 2000; Yamada et al., 2000). This program has a Gabor function as the "mother" wavelet with a central frequency of 7 MHz. The software program also includes a program to calculate the relevant group-velocity curves for the lowest ten modes of the infinite number of Lamb modes that govern the far-field wave propagation in a plate. Figure 2 shows the two lowest modes (fundamental symmetric, So, and anti-symmetric, Ao) superimposed on the WT. This superposition is facilitated by an option that converts the group velocity scale to a time scale using the known exact propagation distance. The group-velocity curves were calculated by use of the same bulk velocities that were used in the finite-element computations (6,320 m/s bulk longitudinal velocity and 3,100 m/s bulk shear velocity). The FEM calculation also uses the material density of 2700 kg/m^3. The color scale in Fig. 2 is a linear scale with red representing the highest-magnitude region of the WT and pink the smallest or zero-magnitude region. The display includes an option to change the color scale (called the color factor) so as to include a greater or lesser portion of the maximum magnitudes in the "red" region. The WT in Fig. 2 has a color-factor (CF) value of 0.8. A color factor of less than 1 (the default value) means that a wider range of the WT peak magnitudes are displayed in red. The converse applies for color factors greater than 1.

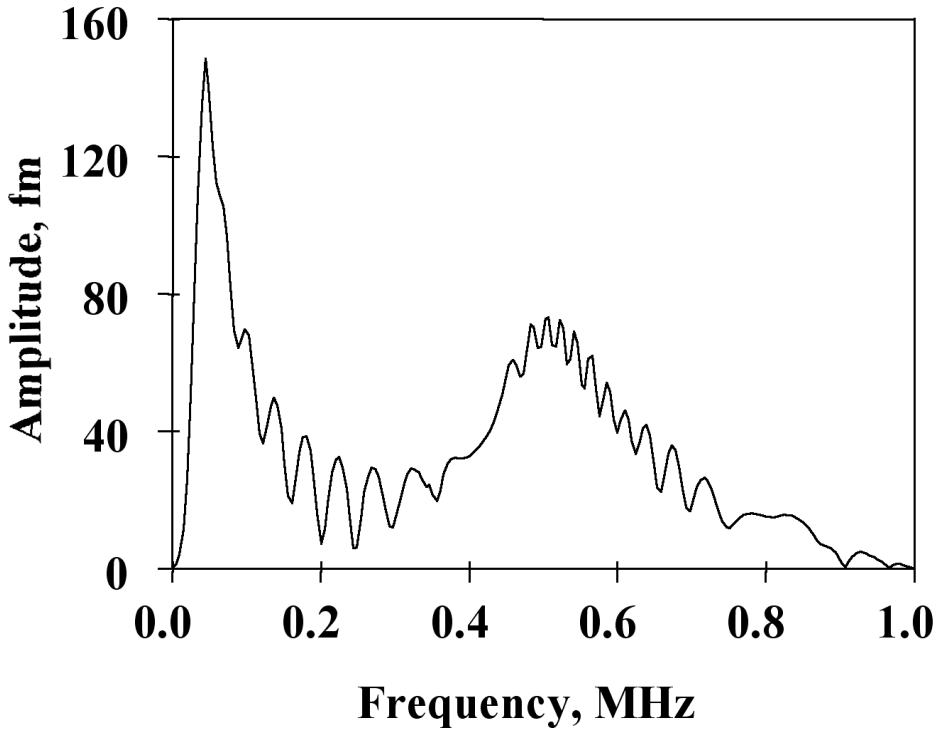

Fig. 3 FFT of the waveform shown in Fig. 2.

Clearly, Fig. 2 shows the presence of AE signal energy in portions of both the fundamental symmetric and anti-symmetric modes. The WT also demonstrates that the AE signal energy is not uniformly distributed between the modes that are present, nor is it uniformly distributed as a function of frequency along each of the dominant modes. These aspects demonstrate a key advantage of the WT as compared to an FFT. The WT shows how the signal energy is distributed as a function of frequency, time (or group velocity), and mode. In contrast, as is well known and illustrated in Fig. 3, the FFT of the same AE signal provides only the frequency content of the whole signal and does not allow one to easily see the modal division or how the intensity of the energy in particular frequency ranges and modes varies as a function of time (or group velocity). Thus, Fig. 2 shows that this AE source has the greatest concentration (most red color) of energy in the anti-symmetric fundamental mode in a frequency range of about 40 to 80 kHz over a range of group velocities from 1.8 to 2.7 mm/μs. Another large amplitude region of the WT is the part of the fundamental symmetric mode in a frequency range from about 500 to 540 kHz, which is centered about a group velocity of about 1.9 mm/μs. With regard to these frequency ranges and group velocities, we point out that the WT algorithm allows the user to select both the frequency resolution and the wavelet size. The effects on the WT results of different choices for these parameters are discussed next.

4. Parameter Selection to Enhance the Resolution/Smoothness of WT Results

The wavelet transform program, AGU-Vallen Wavelet, used in this research is that freely distributed on the World Wide Web (see web site www.vallen.de). There are several parameters that need to be selected prior to the wavelet calculation. Figure 4 shows the setup screen for this wavelet transform. Two parameters must be chosen properly to obtain sufficient resolution of the WT. These parameters are the "Frequency Resolution" and the "Wavelet size". The "Freq. Resolution" gives the frequency interval for the WT calculation, and has a default value of 10

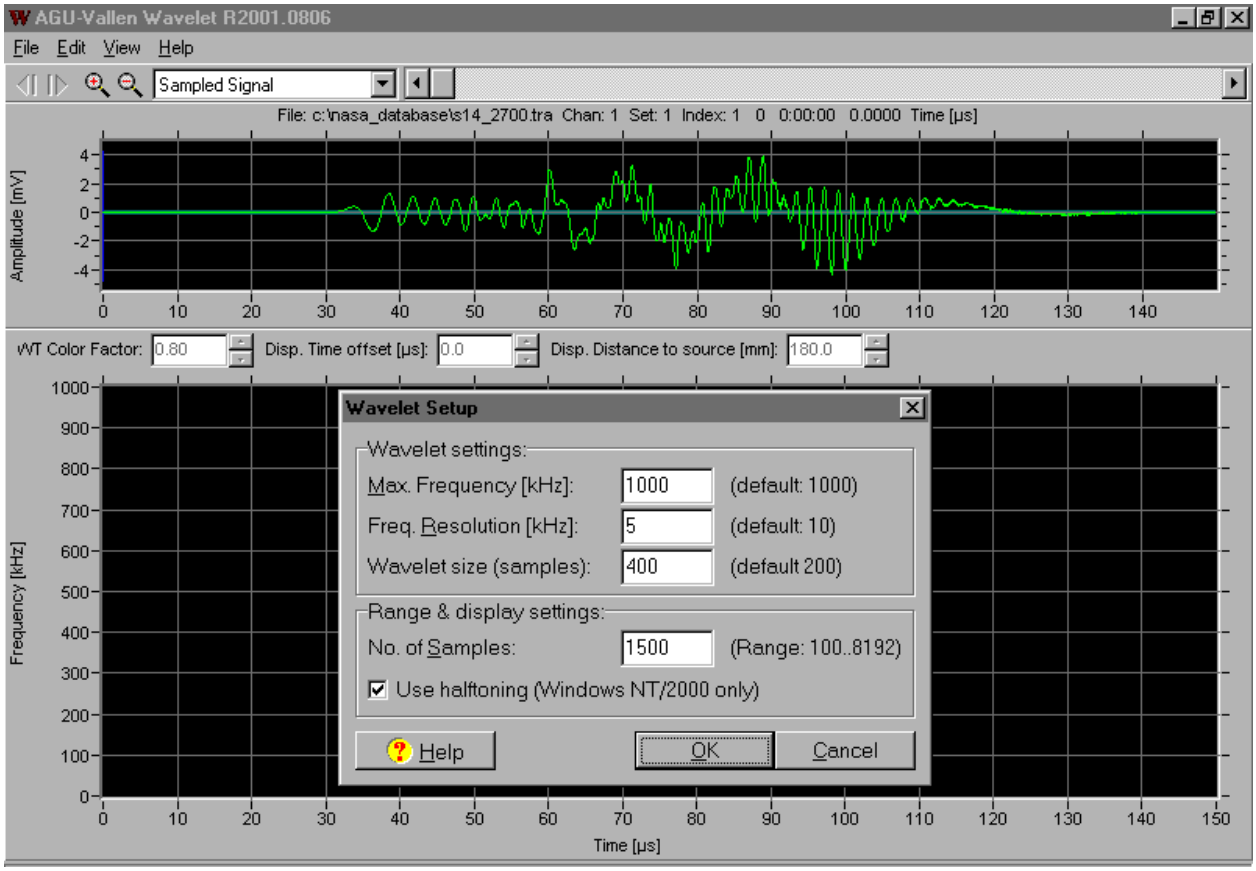

Fig. 4 "Wavelet Setup" screen for AGU-Vallen Wavelet.

kHz. This value is not necessarily the best, as is shown in Fig. 5. In this case the WT was calculated for an in-plane dipole centered at a depth of 0.47 mm in the large plate with a source-to-sensor propagation distance of 180 mm. Figure 5 (a) shows the WT result (CF = 1) with the default value of "Freq. Resolution" of 10 kHz and a "Wavelet size" of 800 samples, and Fig. 5 (b) shows the WT result (CF = 1) using a "Freq. Resolution" of 2 kHz and the same "Wavelet size". Clearly the 10 kHz frequency steps can be seen in Fig. 5 (a). These steps are not present in Fig. 5 (b), which shows a much smoother result. The disadvantage of using the smaller value for the frequency resolution is that the calculation takes longer. For example, on a personal computer with a CPU speed of 0.7 GHz, the WT shown in Fig. 5(a) took about 5 s and that shown in Fig. 5(b) took about 18 s.

The "Wavelet size" has a default value of 200 samples. Figure 6 shows the WT results of the same AE signal used for Fig. 5 with the default value (a) and a size value of 800 samples (b). For this figure the "Freq. Resolution" of 2 kHz was used along with a color factor of 1. It can be seen that the larger "Wavelet size" gives a smoother result. With a larger "Wavelet size" value, the calculation requires more time. To date, our observation has been that an increase in the "Wavelet size" is advisable when the larger amplitudes in the WT are at frequencies below about 100 kHz. Thus, we conclude that it is worthwhile to enhance the resolution and smoothness of the WT results at the cost of slightly longer computational times. For example, on a modern personal computer, the WT shown in Fig. 6 (a) took about 6 s and that shown in Fig. 6 (b) took about 18 s. When WT results were used to extract quantitative results, the parameters were selected to provide better resolution. In other cases lower resolution was used for more qualitative results.

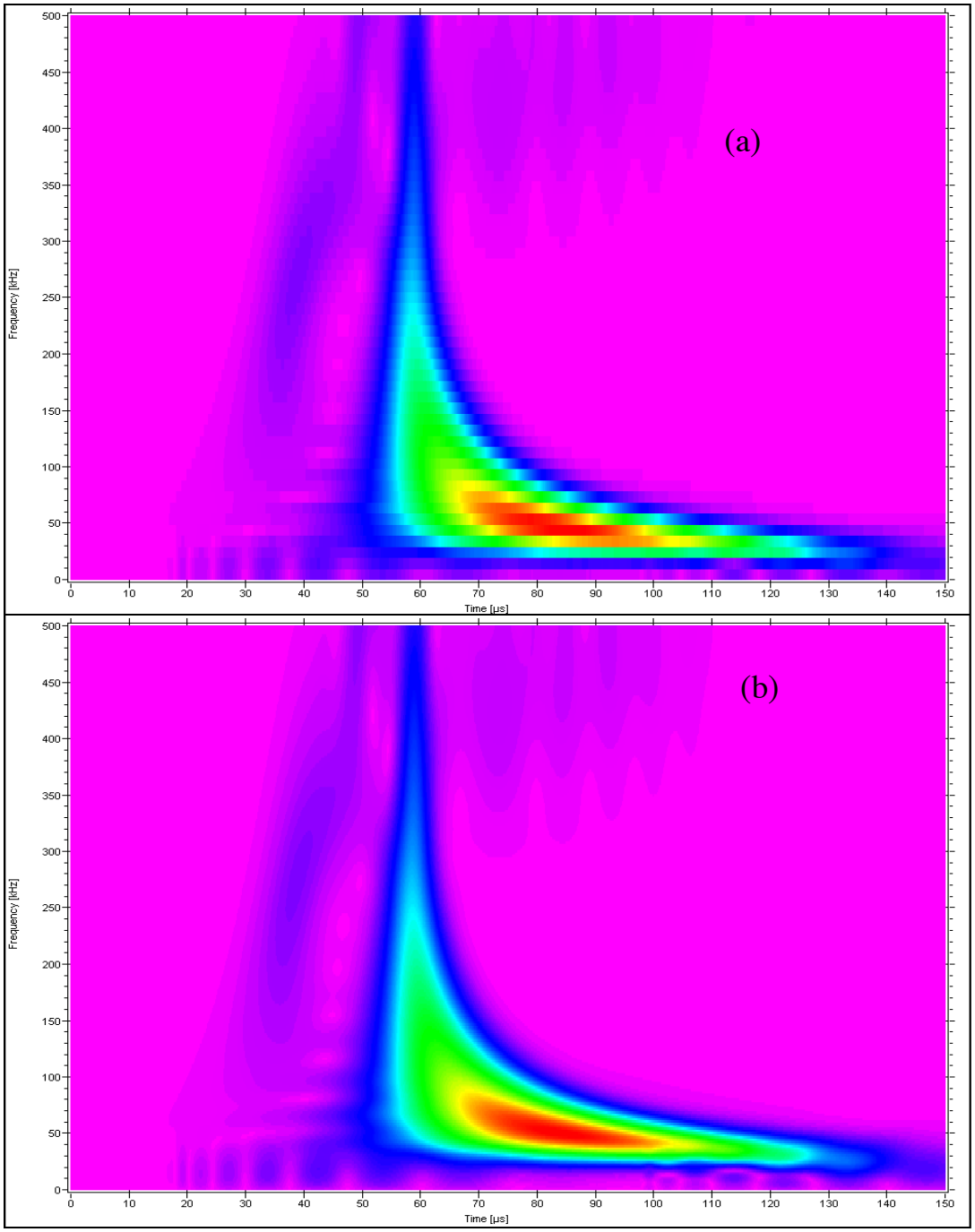

Fig. 5 WT results with low "Frequency resolution" (default) of 10 kHz (a) and high "Frequency resolution" of 2 kHz (b). Both results with a "Wavelet size" of 800 samples. Figures show frequency (0 to 500 kHz) versus time (0 to 150 µs).

5. Correlation of WTs with Source Type (Large Plate)

To begin to study source identification using the FEM database, we first focus on WT results of calculated AE signals at three different propagation distances from a single source. Figure 7 shows the WT results ("Freq. Resolution" of 2 kHz, "Wavelet size" of 600 samples and CF = 1) at the three available distances for an in-plane dipole source (dipole forces are aligned with the direction of propagation to the sensors) at a depth of 1.723 mm in a large plate. This figure

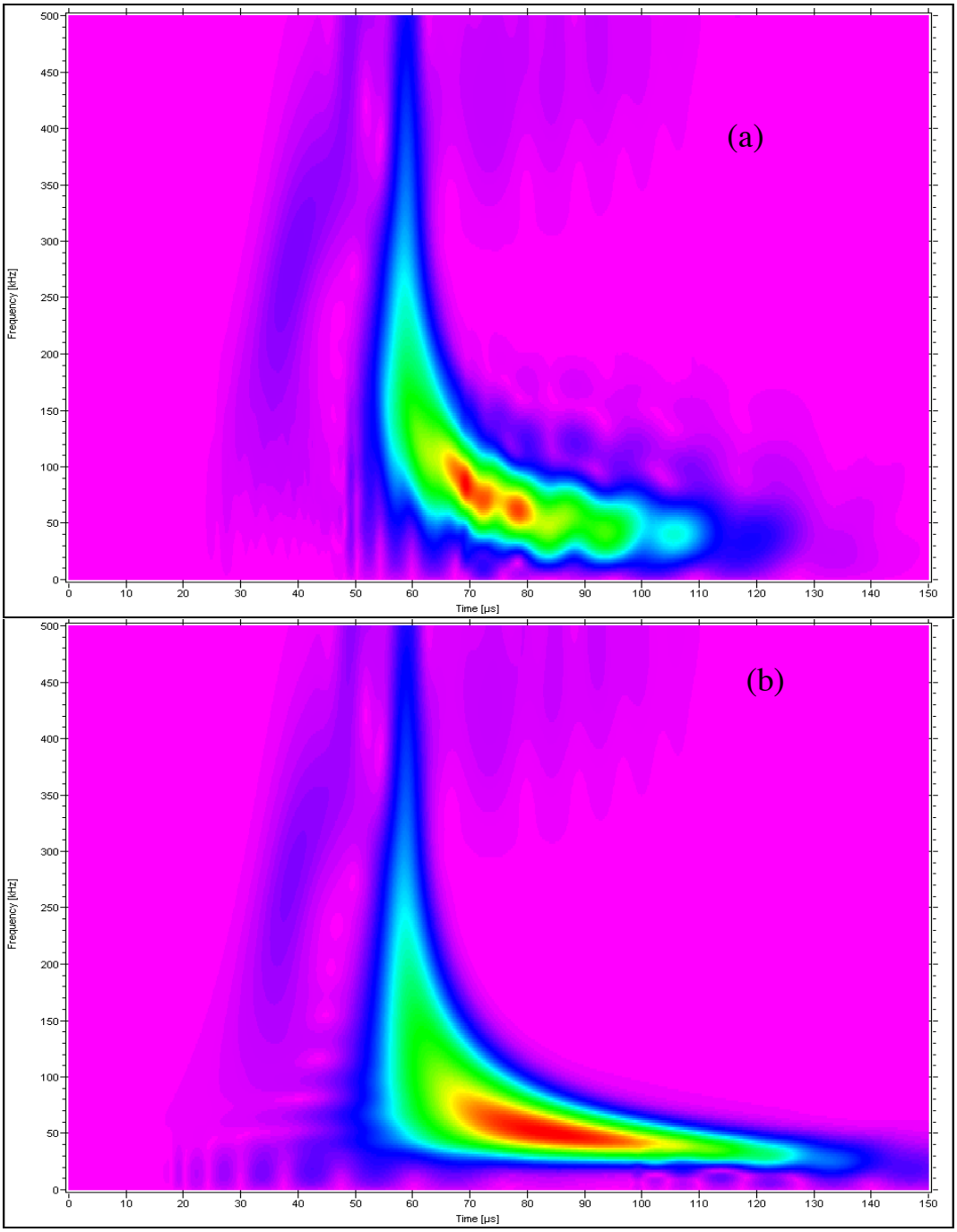

Fig. 6 WT results with small (default) "Wavelet size" of 200 samples (a) and large "Wavelet size" of 800 samples (b). Scales are the same as Fig. 5.

demonstrates that the WT results look very similar at different propagation distances when the time axis has been adjusted for the different distances. Due to this similarity with propagation distance, a limited data set could be extracted from the WT results that potentially shows that these three signals are from the same source. This potential was examined by extracting the WT peak magnitudes at two pairs of frequency and approximate group velocity. The frequencies and approximate group velocities were selected, one from each of the dominant WT magnitude regions of the fundamental modes. The circles in Fig. 7 show the two modal regions where the WT peak magnitudes and associated arrival times were extracted. The selected pairs of fre-

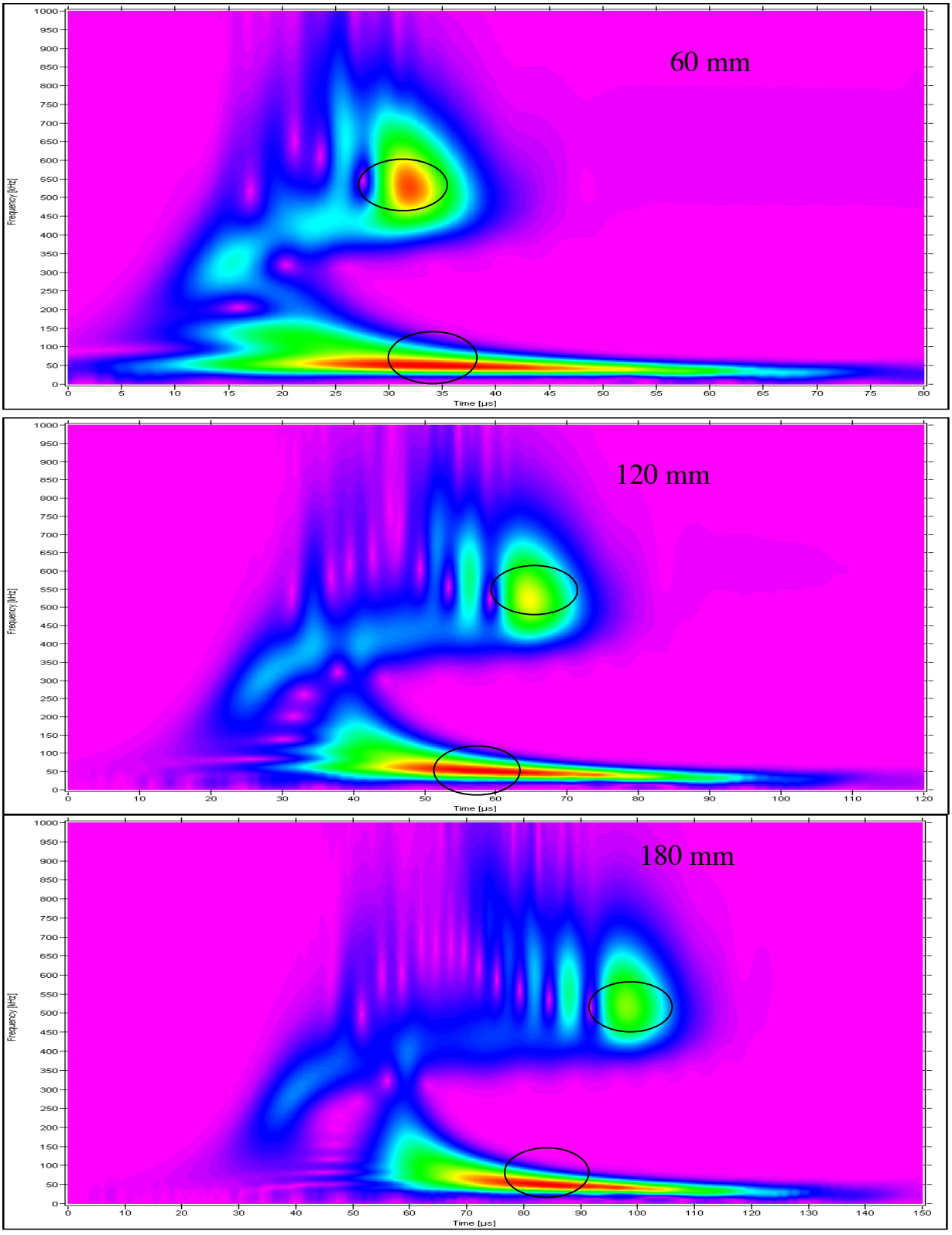

Fig. 7 WT results at three propagation distances 60 mm, 120 mm, and 180 mm for an in-plane dipole source at a depth of 1.723 mm. Circles show approximate regions from which the maximum WT magnitudes and group velocities were extracted at 50 kHz (Ao) and 522 kHz (So). Figures show frequency (0 to 1 MHz) versus time (0 to 80, 120, and 150 µs for the three propagation distances).

Table 1. WT magnitudes (peak value) for specified mode and frequency at indicated group velocity for in-plane dipole source at a depth of 1.723 mm.

	Ao mode at 50 kHz		So mode at 522 kHz		
Propagation distance, mm	Indicated group velocity, mm/μs	WT Magnitude	Indicated group velocity, mm/μs	WT Magnitude	Magnitude ratio, Ao/So
60	1.76	83,454	1.88	77,724	1.1
120	2.02	58,265	1.86	45,904	1.3
180	2.17	46,415	1.84	33,225	1.4

Table 2. WT magnitudes (peak value) for specified mode and frequency at indicated group velocity with sources at a depth of 1.723 mm and a propagation distance of 180 mm.

	Ao mode at 50 kHz		So mode at 522 kHz		
Source Type	Indicated group velocity, mm/μs	WT Magnitude	Indicated group velocity, mm/μs	WT Magnigude	Magnitude ratio, Ao/So
Out-of-plane	2.18	22,819	1.84	35,924	0.64
In-plane	2.17	46,415	1.84	33,225	1.4
Crack initiation	2.14	34,603	1.83	14,546	2.4

quency and group velocity were 50 kHz and about 2.16 mm/μs for the flexural mode (Ao) and 522 kHz and about 1.84 mm/μs for the extensional mode (So). The extraction of the peak WT magnitudes and their arrival times (in the approximate group-velocity region) was facilitated by an option that allows exporting the WT results into spreadsheets. Table 1 shows the extracted results. The indicated group velocity was obtained by dividing the extracted arrival time into the propagation distance from the source epicenter to the sensor location. Table 1 also shows the ratios of the Ao/So peak WT magnitudes at the selected frequencies and group velocities. The use of such a ratio provides a measure that is independent of the original source strength.

Although the Ao/So ratio experiences an increase with increasing propagation distance, this change could be corrected for by developing approximate rates of travel-distance attenuation of the WT magnitudes for the different modes and frequencies being used. Thus, it seems a limited set of data can be extracted (from WT results) that indicates the same source was observed at different propagation distances. However, it should be pointed out that the current dataset studies only the effect of propagation distance in one source-radiation direction (and the direction 180 degrees opposed; a symmetrical direction). Since a source in a plate emits different amounts of energy of the bulk modes in different radiation directions, future research should check the above conclusions (for source identification) when the propagation distance varies along with the two-dimensional radiation direction in the plane of the plate. Due to the typical symmetries of radiation patterns of sources aligned with the plate coordinate axes, this check will need to be done for only one quadrant rather than for a full 360 degrees.

To extend the study of extraction of a limited database for AE source identification from WT results, the next focus was on three different source types and their signals at a fixed propagation distance of 180 mm. Figure 8 shows (CF = 1) the WTs for an in-plane dipole (a), out-of-plane dipole (b), and a microcrack initiation (c) with all the sources centered at 1.723 mm below the top surface. These WTs were calculated with a "Frequency Resolution" (FR) of 2 kHz and a "Wavelet size" (WS) of 600 samples. Following the same procedure that was used with Fig. 7 to obtain the data in Table 1, the data shown in Table 2 were obtained from the WTs in Fig. 8. Again circles have been drawn in Fig. 8 about the regions from which the modes, approximate group velocities and frequencies were selected. Examination of Table 2 indicates that the sig-

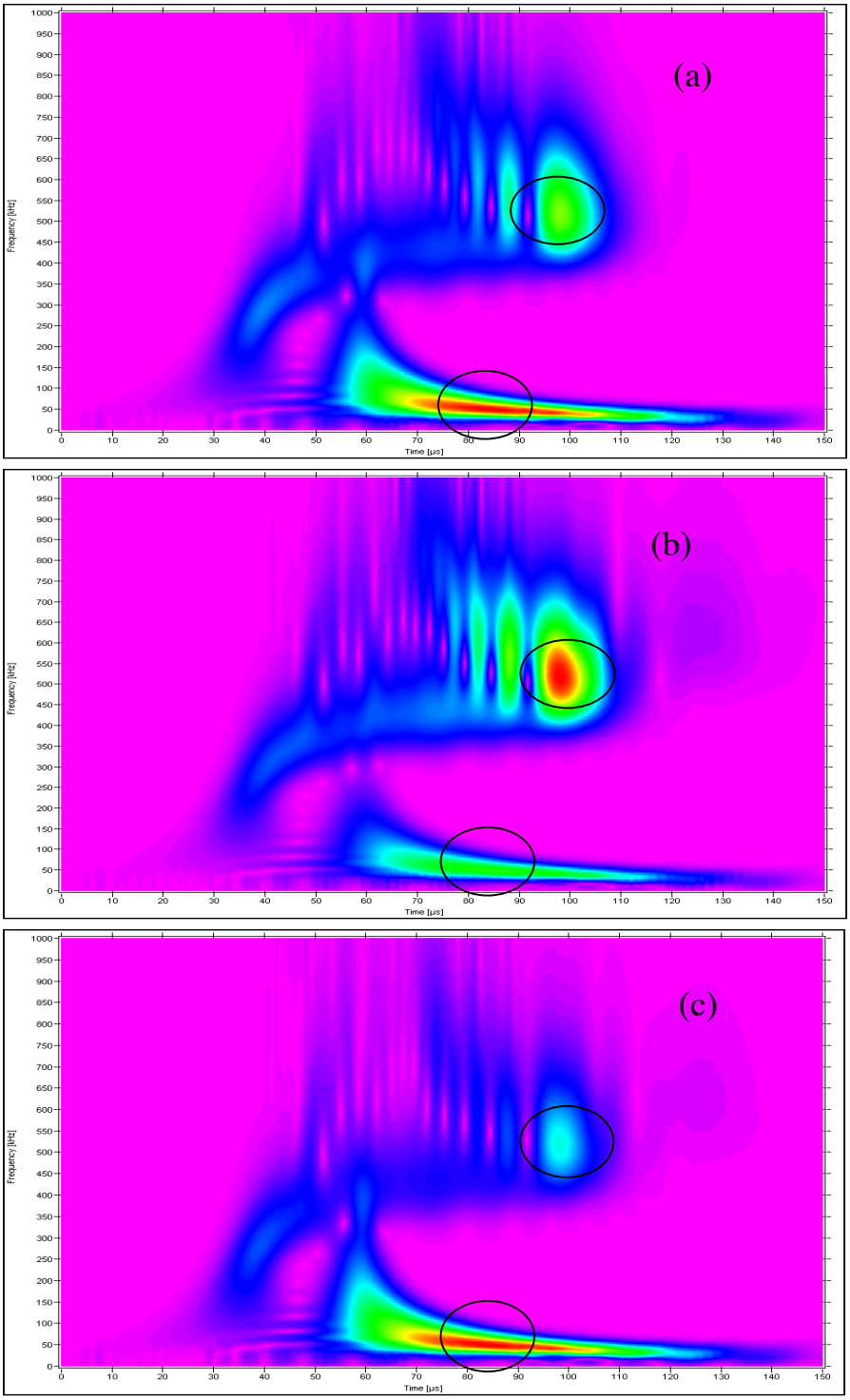

Fig. 8. WT results from out-of-plane displacement signals for three different source types: (a) in-plane dipole, (b) out-of-plane dipole and (c) crack initiation. Sources are all at a depth of 1.723 mm. Circles show approximate regions from which the maximum WT magnitudes and group velocities were extracted at 50 kHz (Ao) and 522 kHz (So). Figures show frequency (0 to 1 MHz) versus time (0 to 150 µs) for the signals at 180 mm propagation distance.

nificant changes of the simple Ao/So ratio potentially could be used for source identification. The out-of-plane dipole source had the smallest ratio, and the crack-initiation source had the largest ratio.

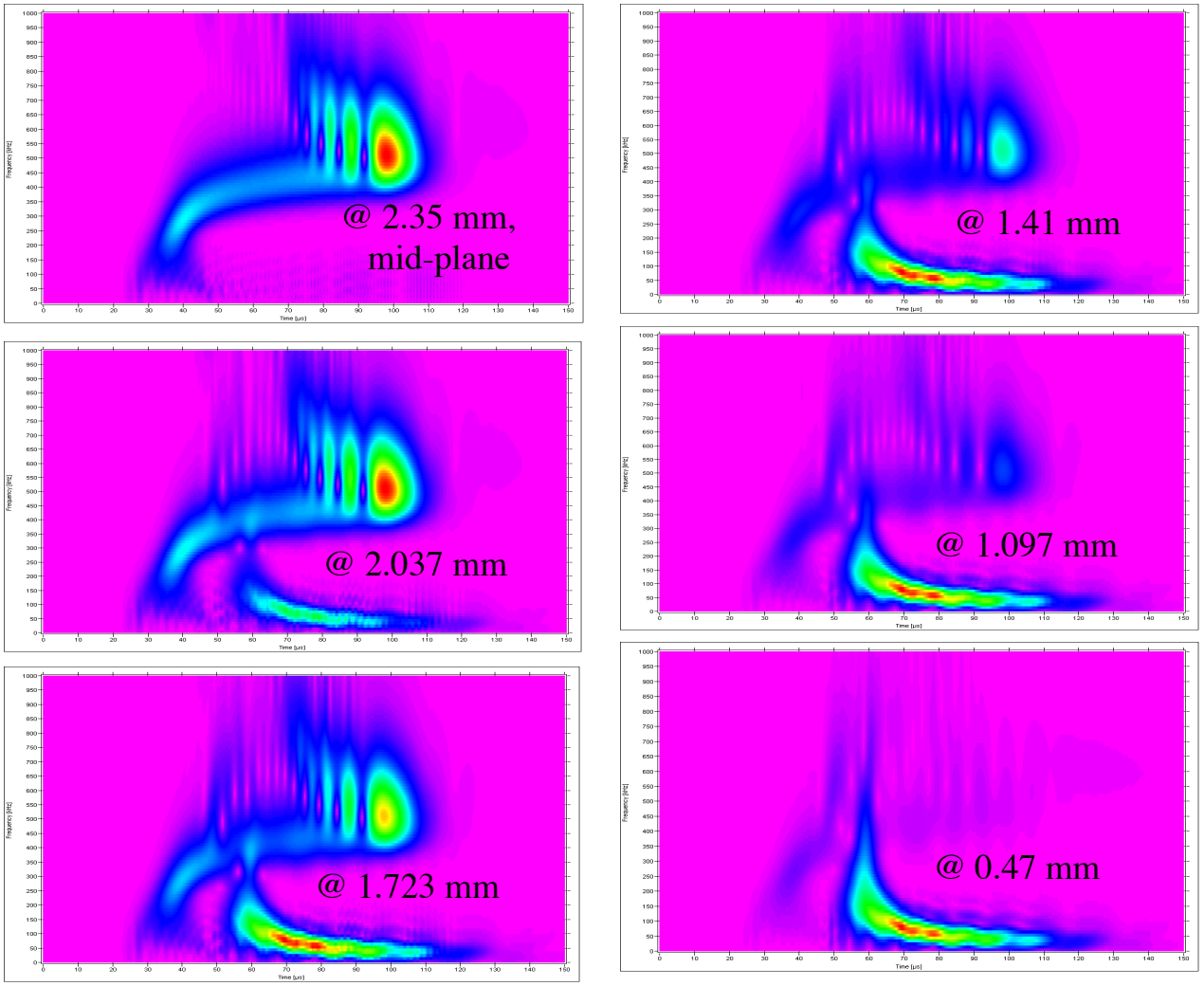

Fig. 9. WT plots as a function of the indicated source depths below the plate top surface. The source was an in-plane dipole with a 180 mm propagation distance. Figures show frequency (0 to 1 MHz) versus time (0 to 150 μs).

Examination of WT results for a single source type as a function of source depth reveals some potential difficulties in the approach suggested above. Figure 9 demonstrates the changes in WTs (with default values and CF = 1 for the AE signals at 180 mm) for an in-plane dipole as a function of the depth of the source below the top surface of the plate. Even a casual examination of the results in this figure shows that the WT result varies substantially as the depth of the source changes. For the source located at the mid-plane (at 2.35 mm) the fundamental symmetric (extensional) mode dominates. As the source is moved closer to the surface, it is clear that the energy carried in the extensional mode decreases and most of the energy is carried in the fundamental anti-symmetric (flexural) mode. This dependence of the dominant Lamb modes and associated frequencies can also be seen in the signal waveforms and their FFTs. These results are shown in Fig. 10 as a function of source depth for the same series of depths. The dependence of the WT results on source depth also is apparent for the out-of-plane dipole source and the more complicated microcrack initiation source. These WT results (default parameters and CF = 1) for the AE signals at 180 mm are shown in Fig. 11 for two different depths (0.783 and 1.723 mm).

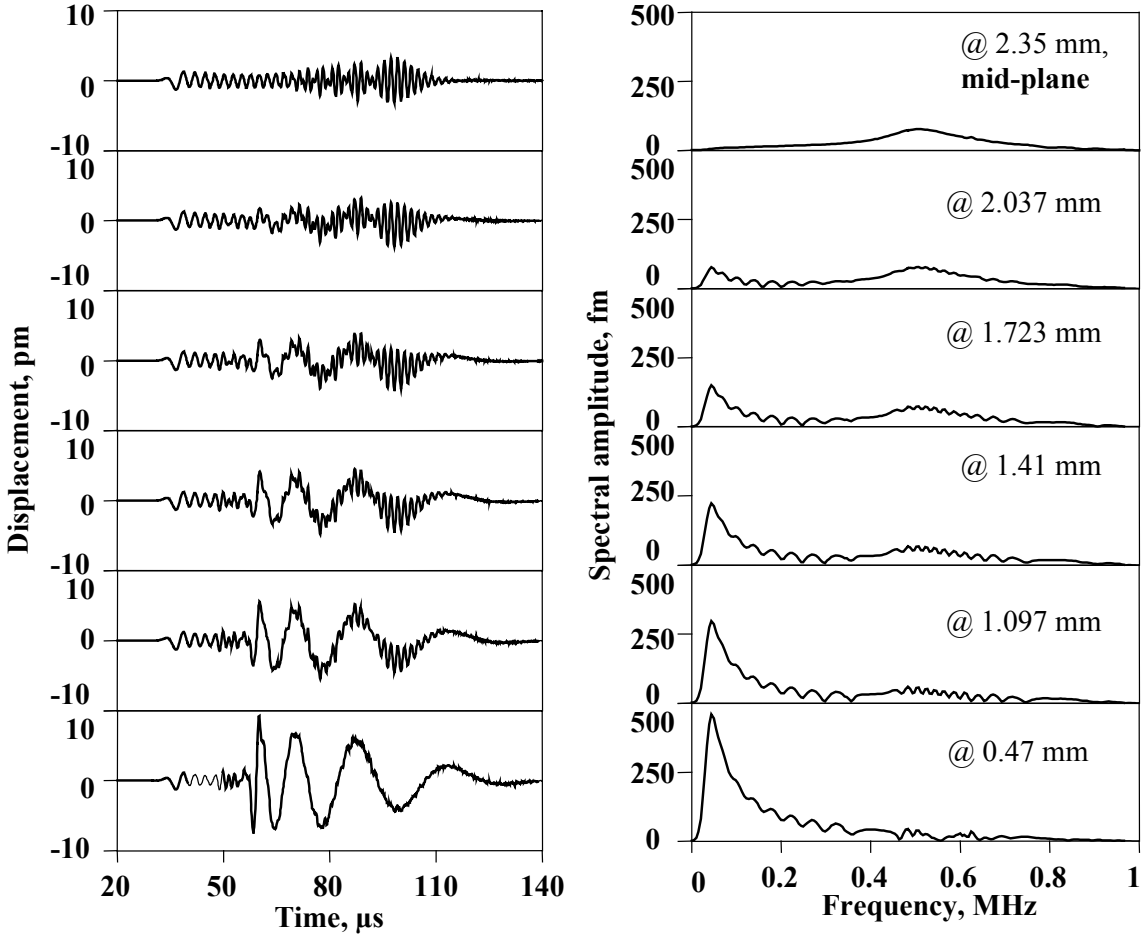

Fig. 10. Calculated AE signals with corresponding FFTs (in the same sequence top to bottom) for same cases shown in Fig. 9.

The possibility of extracting from WTs (of the out-of-plane displacement signals) a more limited data set to uniquely identify the different AE sources certainly exists. However, it is complicated by the dependence of the AE signals and their WTs on the depth of the sources. There are two primary reasons for this complication. First, the Ao/So ratio changes not just with source type but with source depth. The primary change (for the three source types considered) that takes place when the depth of a source changes is a transfer of more energy to either the extensional mode or the flexural mode from the alternate mode. Thus, it does not seem possible to extract simple Ao/So ratio information, such as in Tables 1 and 2, from the WTs that is unique to a particular source type. Second, since at a fixed depth there are clear differences between source types (see Fig. 8 and Table 2), it is likely, as a consequence of the transfer of energy between modes, that two different sources at two different source depths could have very similar WTs. This is in fact the case, as Figs. 12 and 13 show (calculated using default WT parameters) for signals at 180 mm from the sources. Figure 12 shows (CF = 1) that a microcrack initiation source (a) at a depth of 0.783 mm has nearly the same WT as an in-plane dipole source (b) at a depth of 0.47 mm. Figure 13 demonstrates (CF = 1) the close WT similarities between an out-of-plane dipole source (a) at a depth of 1.723 mm and an in-plane dipole source (b) at a depth of 2.037 mm.

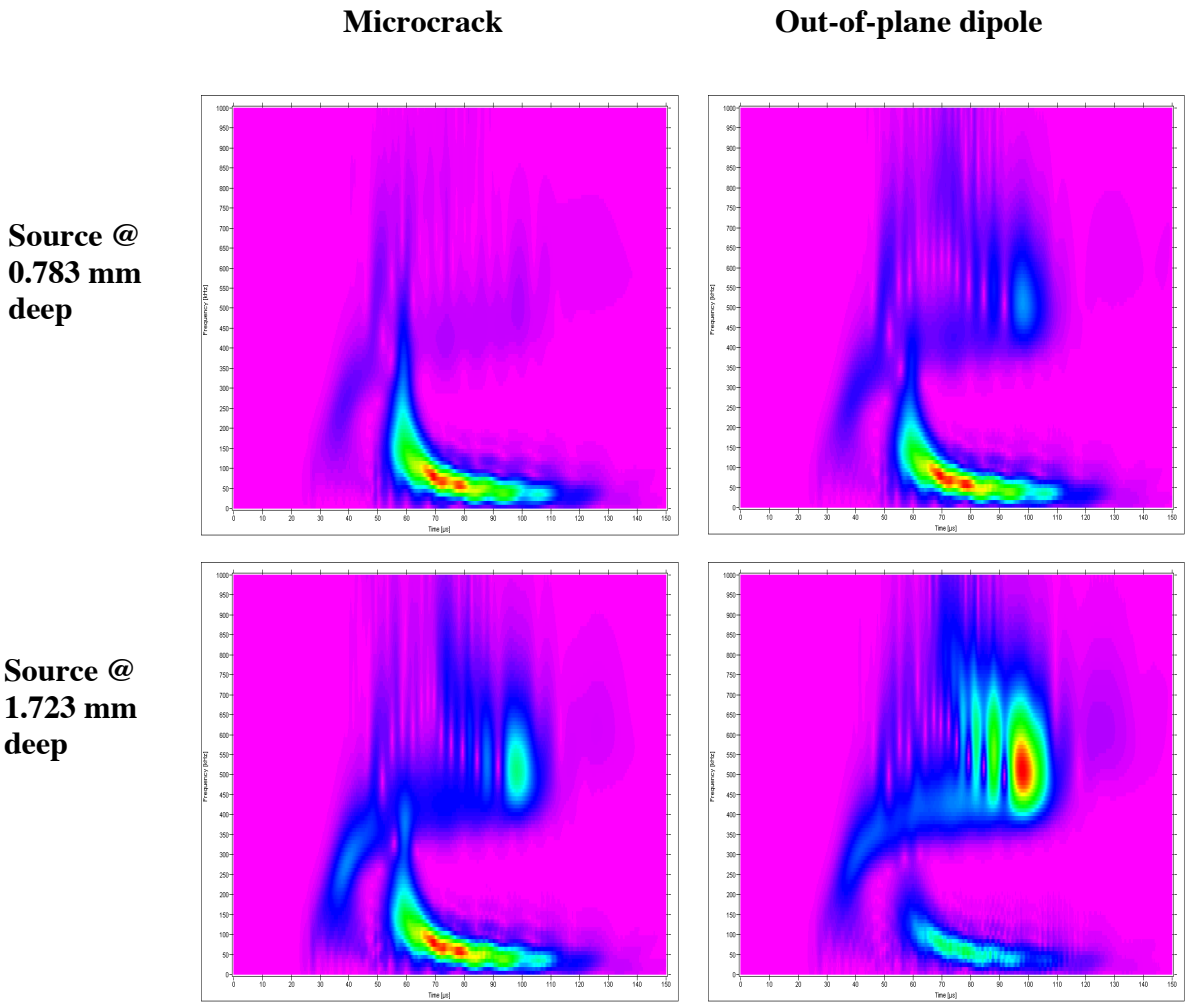

Fig. 11. WT plots showing the distinctions between a microcrack initiation source and an out-of-plane dipole compared at the same two different source depths and at 180 mm propagation distance. Plots show frequency (0 to 1 MHz) versus time (0 to 150 μs).

One might consider whether the lower-magnitude regions of the WTs in Figs. 12 and 13 might provide suitable simple features that would distinguish these sources. This might be the case as shown in Fig. 14, which shows WTs for the same signals used for Fig. 13 calculated with WS = 600 samples and FR = 2 kHz. Also in Fig. 14, the CF was set at 0.8 to provide a wider-magnitude range for the red color region. This setting of the CF effectively shows more features of the lower-magnitude parts of the WTs. The arrows in Fig. 14 point to regions where the WT of the in-plane dipole (b) has a larger magnitude than the WT of the out-of-plane dipole (a). But, this aspect that shows up very well in the FEM modeled data may not be nearly as clear when the typical signal-to-noise ratios of real AE signals are considered. In the modeled case, data has little or no apparent noise. Thus, examining differences in regions of lower WT magnitude may not be a practical solution for real AE signals.

To examine the depth effects more systematically and quantitatively, high-resolution WTs were calculated from signals at a propagation distance of 180 mm for the different source types and depths in the available database. The WT peak magnitudes at two pairs of frequency and approximate group velocity were then extracted for each case. The frequencies and approximate

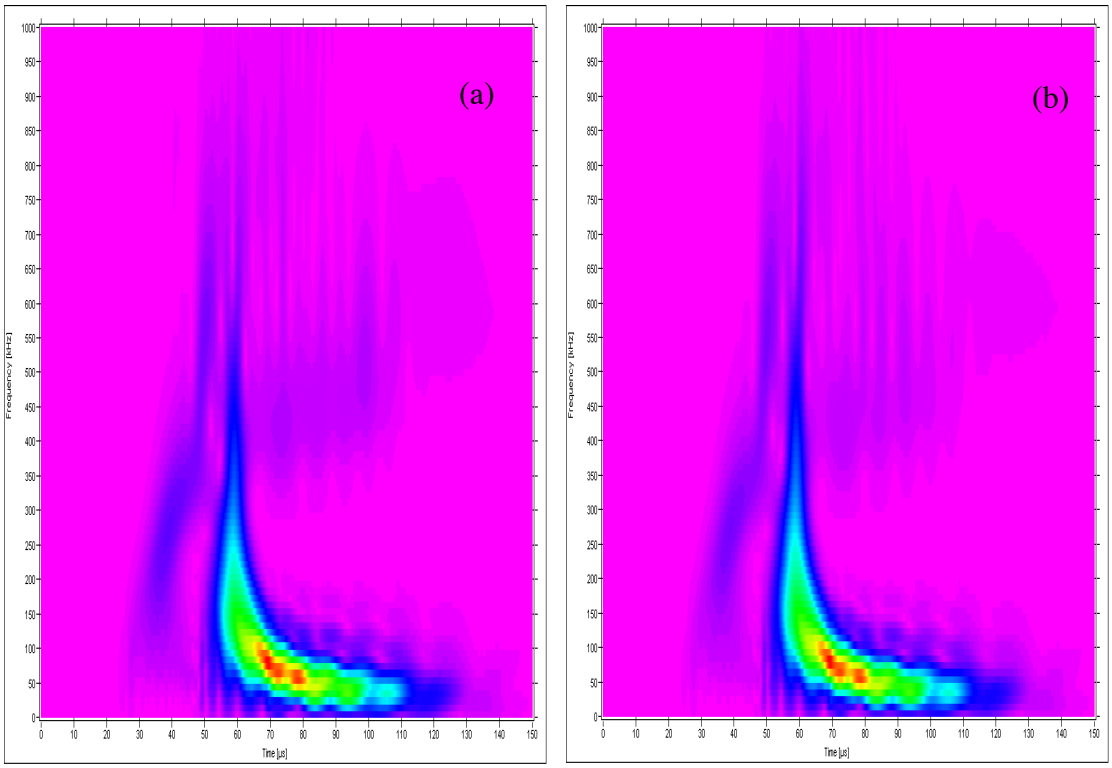

Fig. 12. WT plots showing the similarities for two different source types at different depths. At 180 mm propagation distance. Microcrack initiation (a) at 0.783 mm depth and in-plane dipole (b) at 0.470 mm depth. Plots show frequency (0 to 1 MHz) versus time (0 to 150 µs).

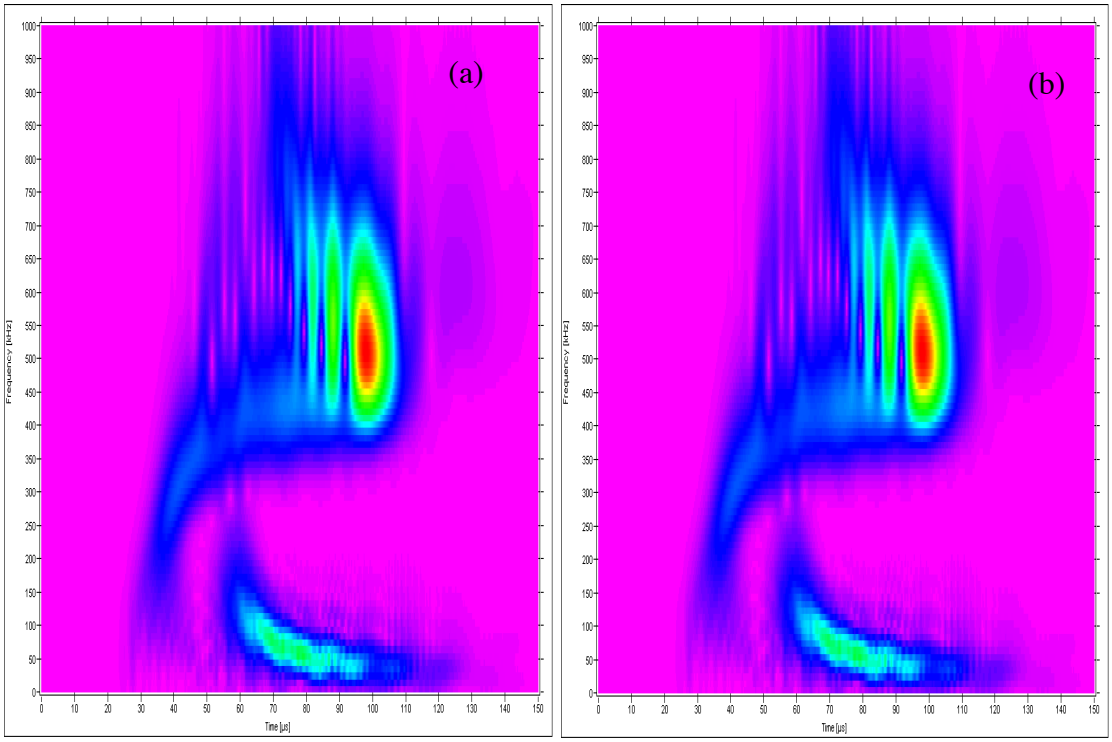

Fig. 13. WT plots show the similarities for two different source types at different depths. At 180 mm propagation distance. Out-of-plane dipole (a) at 1.723 mm depth and in-plane dipole (b) at 2.037 mm depth. Plots show frequency (0 to 1 MHz) versus time (0 to 150 µs).

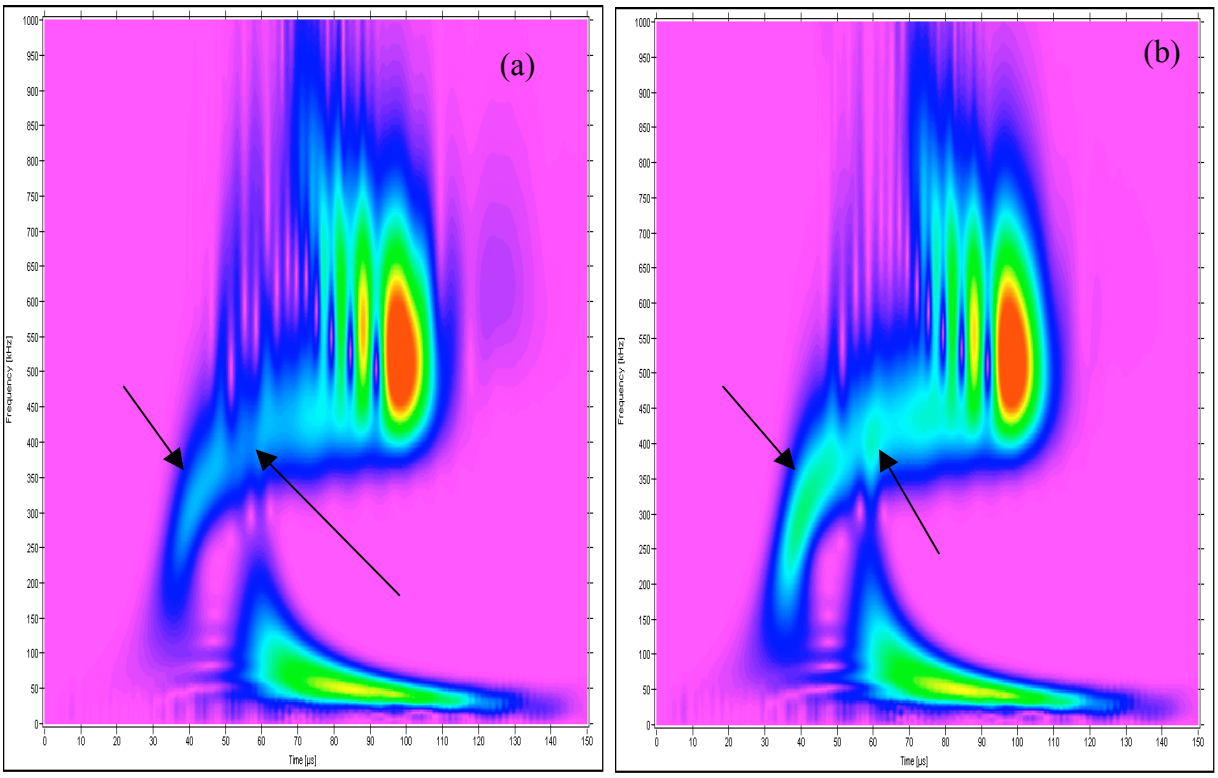

Fig. 14. Same cases and scales as Fig. 13 with color factor changed to 0.8 to examine differences in WTs in their lower magnitude regions. Arrows point to higher magnitude regions in the in-plane dipole (b) versus the out-of-plane dipole (a).

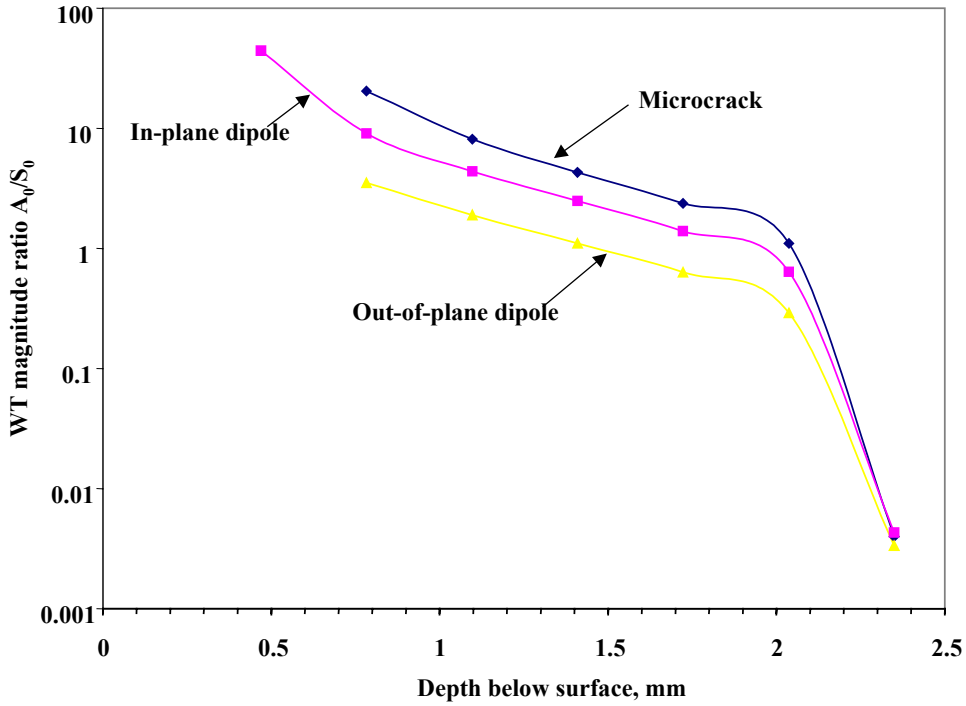

Fig. 15. Ao/So ratio of peak WT magnitudes versus AE source depth for the microcrack initiation, in-plane dipole and out-of-plane dipole sources at 180 mm propagation distance. Peak magnitudes at 50 kHz and approximate group velocity of 2.16 mm/µs for Ao and at 522 kHz and approximate group velocity of 1.84 mm/µs for So.

Table 3a. WT magnitudes (peak value) for specified mode and frequency at indicated group velocity for in-plane dipole source at 180 mm. (Note * indicates a peak was not present)

	Ao mode at 50 kHz			So mode at 522 kHz			
Source depth, mm	Indicated group velocity, mm/μs	WT Magnitude		Indicated group velocity, mm/μs	WT Magnitude		Magnitude ratio, Ao/So
2.35	2.18	160*		1.84	37,124		0.0043
2.037	2.18	23,104		1.84	36,138		0.64
1.723	2.17	46,415		1.84	33,225		1.4
1.41	2.14	70,427		1.84	28,398		2.5
1.097	2.14	95,209		1.83	21,738		4.4
0.783	2.14	121,144		1.83	13,331		9.1
0.47	2.15	148,578		1.82	3,357		44

Table 3b. WT magnitudes (peak value) for specified mode and frequency at indicated group velocity for microcrack initiation at 180 mm. (Note * indicates a peak was not present)

	Ao mode at 50 kHz			So mode at 522 kHz			
Source depth, mm	Indicated group veloicty, mm/μs	WT Magnitude		Indicated group velocity, mm/μs	WT Magnitude		Magnitude ratio, Ao/So
2.35	2.14	166*		1.84	16,535		0.004
2.037	2.14	17,248		1.84	16,035		1.1
1.723	2.14	34,603		1.83	14,546		2.4
1.41	2.18	52,296		1.83	12,084		4.3
1.097	2.14	70,490		1.83	8,669		8.1

Table 3c. WT magnitudes (peak value) for specified mode and frequency at indicated group velocity for out-of-plane dipole at 180 mm.

	Ao mode at 50 kHz			So mode at 522 kHz			
Source depth, mm	Indicated group velocity, mm/μs	WT Magnitude		Indicated group velocity, mm/μs	WT Magnitude		Magnitude ratio, Ao/So
2.35	2.16	132.7		1.84	39,605		0.0034
2.037	2.14	11,343		1.84	38,676		0.29
1.723	2.18	22,819		1.84	35,924		0.64
1.41	2.14	34,843		1.84	31,402		1.1
1.097	2.14	47,510		1.84	25,177		1.9
0.783	2.14	61,099		1.84	17,365		3.5

group velocities selected were those from the dominant WT magnitude regions of both fundamental modes. The selected values for the flexural mode (Ao) were 50 kHz and about 2.16 mm/μs. For the extensional mode (So), the values were 522 kHz and about 1.84 mm/μs. Then, as before, at each frequency the maximum WT magnitude and its arrival time were determined near the selected approximate group velocities. For certain cases the magnitudes of the WT are relatively small at the selected frequency and approximate group velocity, and in some cases the WT did not have a clear maximum in the approximate group-velocity region. In these latter cases, the WT magnitude at the selected frequency was selected at the same arrival time that the peak magnitude occurred when the same source type was at the nearest depth where the WT as a function of time had a true maximum in that region. The values determined are shown in Tables 3a, b and c for the three different source types. Also, these tables include the calculated magnitude ratio Ao/So for the range of source depths and source types. Figure 15 shows a plot of Ao/So versus source depth with the source type as a parameter. It is reasonable to conclude that there is a definite ordering of the Ao/So ratio as function of source depth. The microcrack initia-

tion source results in the highest values and the out-of-plane dipole has the lowest values, with the in-plane dipole source in between. The relative differences between the ratios at a fixed depth are not small, since the ratio scale in the figure is logarithmic. At the mid-plane depth (2.35 mm), the ratio values are likely not reliable due to the very small WT magnitudes for the Ao mode. Also, these Ao values were in most cases arbitrarily selected as described above since the Ao mode did not have a peak value for the approximate group velocity region of the mode.

It is clear in the case of experimental data when the source depth is unknown that the Ao/So ratio alone will not uniquely define a source type. But, if one considers the data in Fig. 15 to be that for a radiation direction of zero degrees, then it may be possible that results of Ao/So ratios from other radiation directions could provide sufficient additional information to uniquely identify the source type. This expectation, not unlike the approach of Buttle and Scruby (1990a), uses the fact that the radiation pattern is different for different source types. Since in experimental situations typically three or four sensors are hit when two-dimensional source location is determined (a prerequisite for the above approach, since the selected approximate group velocity needs to be converted to an approximate arrival time), signals are typically available in several two-dimensional radiation directions. For these different radiation directions, the Ao/So ratio could be extracted from WTs of the signals. These ratios could then be compared as a function of the radiation angle with modeled results of the Ao/So ratio versus radiation angle determined for different source types and depths. This method could possibly add sufficient information to uniquely identify the source type and source depth. Based upon these observations in future research we expect to examine the above approach with a FEM database that includes other radiation directions.

The application to experimental AE data of the Ao/So ratio approach will likely experience difficulties when the source is located very near the plate surfaces or very near the plate's mid-plane. As the first and last rows of Tables 3a, b and c show, in these cases either the Ao or So WT-based magnitude is small, and they do not always have a local maximum (at a given frequency and associated approximate group velocity). Thus, for experimental data from sources near the mid-plane, effects of low signal-to-noise ratios will likely eliminate the possibility of calculating meaningful Ao/So ratios. A possible solution to this problem might be to focus on the single dominant mode for these source-depth cases. For example, for a source located near or at the mid-plane of the plate two or more frequencies and associated approximate group velocities could be selected from the So mode. At these frequencies and velocities the maximum magnitudes of the WT could be determined within the So mode. Then ratios such as So (at 522 kHz) to So (at say 325 kHz) could be calculated. It is possible that this ratio or other appropriate ones might result in distinguishing different source types located near the plate mid-plane. And for a source located near the plate surfaces, a ratio from two frequencies of the Ao mode could be used. Hence, in future research we expect to examine such an approach using the current FEM database extended to include other source types, such as a shear source, and various radiation angles.

6. WT Data Subsets for Source Identification in Specimens with Nearby Edges

When the lateral size of the test specimen is decreased so that nearby edges are present, the AE signals and their WTs become much more complicated. This result is clearly seen in Fig. 16, which compares WTs of the AE signals (40 kHz high-pass) at 180 mm from in-plane and out-of-plane dipole sources in the small coupon specimen (Fig. 16(a)) and the large specimen (Fig. 16(b)) both at a depth of 1.723 mm. Figure 17(a) also shows as a function of propagation dis-

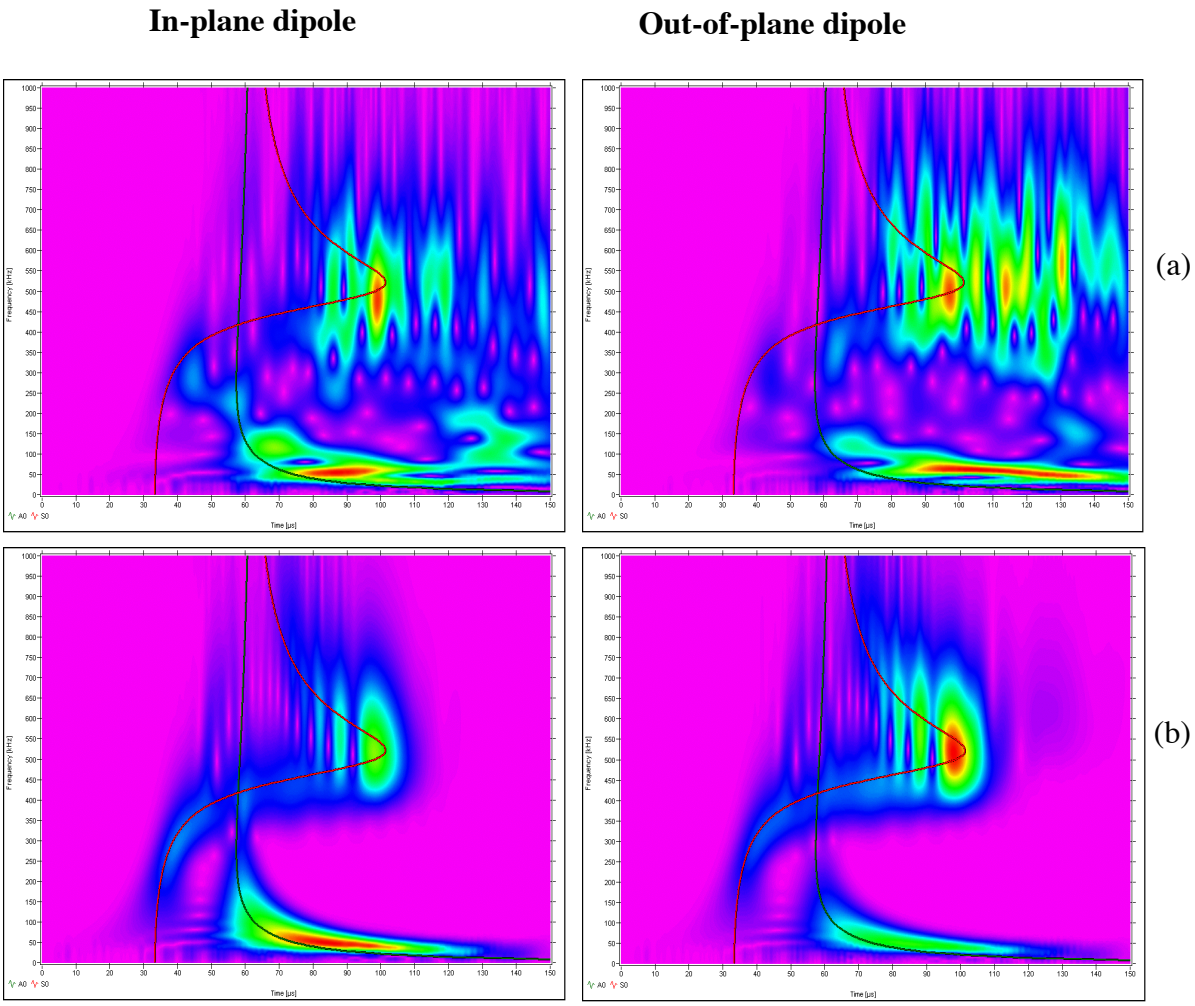

Fig. 16. WT results (40 kHz high-pass AE signals) for coupon specimen (a) with multiple edge reflections compared to large specimen (b) without edge reflections. Results shown for an in-plane dipole source and an out-of-plane dipole source with a propagation distance of 180 mm. Sources centered at 1.723 mm below the top surface of the plate. Frequency (0 to 1 MHz) versus time (0 to 150 μs). Superimposed fundamental modes shown.

tance the significant distortion in the WT results (of AE signals from an in-plane dipole) for the coupon specimen compared to the large specimen (Fig. 17(b)) with sources at a depth of 1.723 mm. The distribution of signal energy in the coupon as shown in Figs. 16(a) and 17(a) does not clearly follow the shapes of the superimposed fundamental Lamb-mode curves from the dispersion relations. Thus the extension of the possible extraction approaches proposed for source identification in the large plate is not straightforward for the coupon specimen. Further, since the distortion of the WT results is due to edge reflections (sides and at later times the specimen ends), moving the source from side-to-side across the 25.4 mm dimension of the coupon specimen will change the reflections in the AE signals. These source-position changes will also change the associated WTs as shown in Fig. 18 with superimposed fundamental modes. This figure compares the WTs for in-plane dipole sources as a function of the transverse position of the AE source. In Fig. 18(a), the source was located half-way across the specimen at 12.7 mm from the coupon side edge. In Figs. 18(b) and 18(c), the source was successively at 6.13 mm and 3.31 mm from the coupon side edge. The WTs (CF = 1, WS = 600) in these figures were calculated from the AE signals at 180 mm from the sources. The source depth was 2.35 mm. The

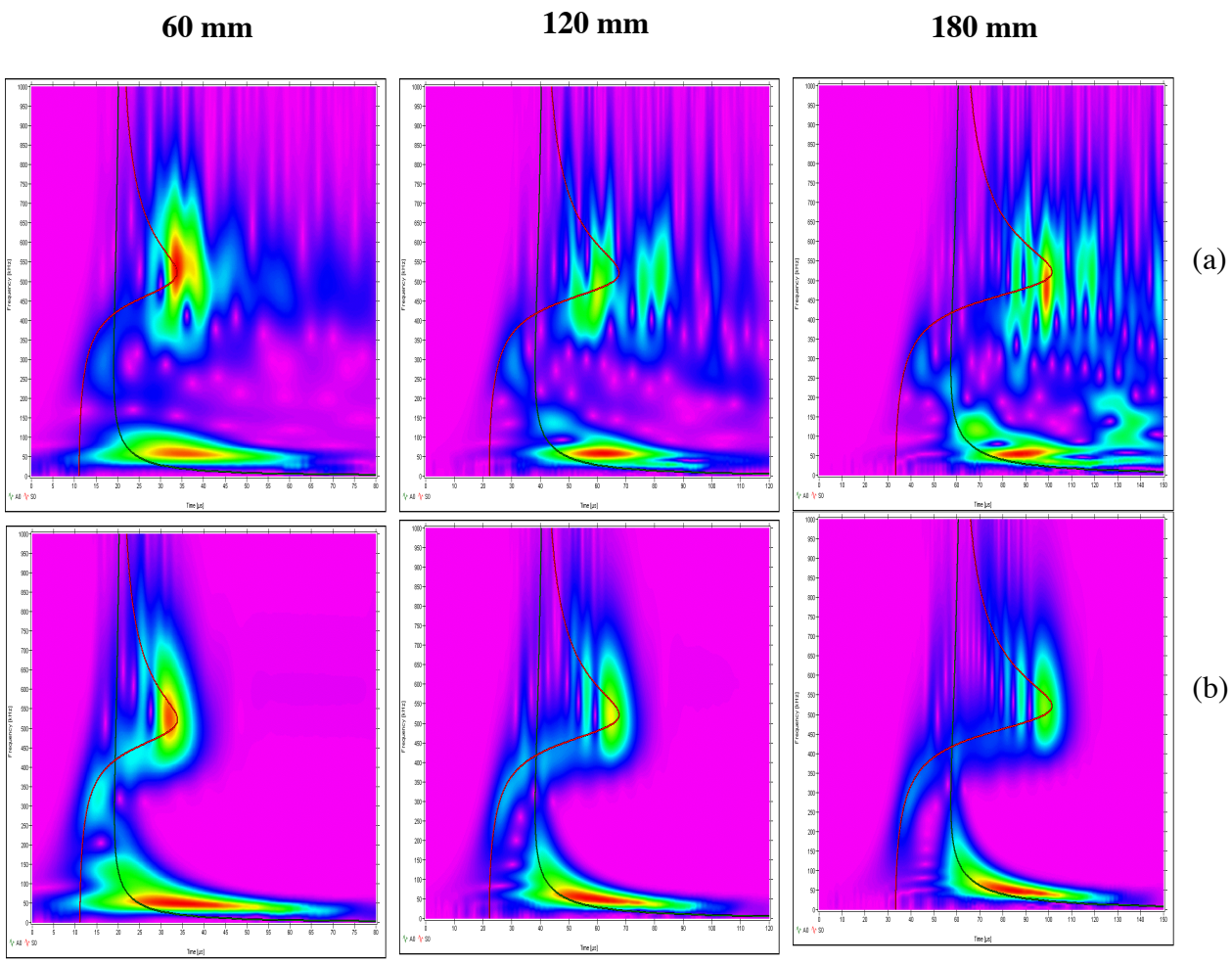

Fig. 17. WT results (40 kHz high-pass AE signals) for coupon specimen (a) with multiple edge reflections contrasted to large specimen (b) without edge reflections at three propagation distances: 60 mm, 120 mm, and 180 mm. Source in-plane dipole centered at a depth of 1.723 mm below the top surface of the plate. Frequency (0 to 1 MHz) versus time (0 to 80, 120, and 150 μs with increasing propagation distance). Superimposed fundamental modes shown

current coupon database, except for the case illustrated in Fig. 18, does not include the side-to-side variation of the source position.

We believe the possible use of a WT for source identification in small specimens needs study because researchers use such specimens. Thus the necessary FEM database should be developed. But, it is prudent in the case of source identification that such studies be done after the potential difficulty of the dependence of the AE signals on the depth of the source is resolved. If the resolution of source depth difficulties requires the use of AE signals in several directions of radiation, then source identification in the small coupon specimen will likely require an alternate approach. This conclusion follows from the fact that in the coupon specimen far-field signals will not be available for different radiation directions. Researchers might be forced to use the bulk wave approach mentioned earlier (Buttle and Scruby, 1990a) if information from different propagation directions is required. This approach has been used in a 8-mm-thick coupon by placing the sensors in very close proximity to known crack tips (Buttle and Scruby, 1990b). Reducing the coupon thickness will eventually result in a sample that is too thin to allow one to

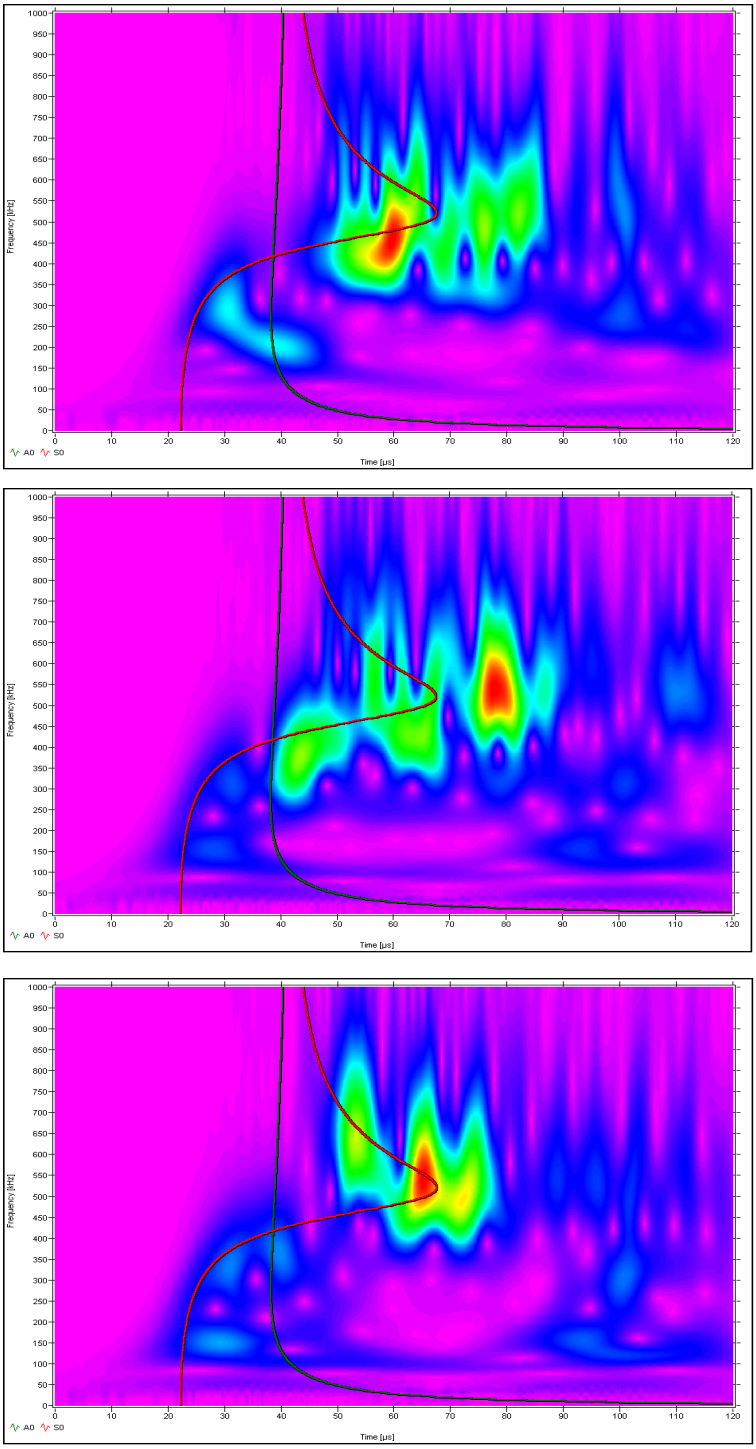

Fig. 18. Comparison of WT results (40 kHz high-pass AE signals) as a function of transverse position of the in-plane dipole source in the coupon specimen. The WTs with superimposed fundamental modes were calculated from the displacement signals at 120 mm for the mid-plane depth source. The sources were located half-way across the specimen (a) at 12.7 mm from the edge, (b) at 6.13 mm from the edge, and (c) at 3.31 mm from the edge. Plots show frequency (0 to 1 MHz) versus time (0 to 120 µs).

distinguish the bulk-wave arrivals from sample surface reflections. Also, to practice the bulk-wave approach, the AE sources of interest must be located in a small known region.

7. Conclusions

A. Source Identification–Large Plates

- For the 4.7 mm aluminum plate thickness of the current FEM database, a potentially useful parameter for source identification has been found. Using a separate selected frequency and approximate group velocity for each fundamental mode, the WT coefficients (usually local maxima for the frequency and group velocity) can be combined to form an Ao/So magnitude ratio. This ratio was found to distinguish different source types when the sources were all centered at the same depth below the plate surface and with the same propagation distance.
- But, since the values of this ratio overlap for different source types at different depths, it is not possible to uniquely identify the source type with this small set of WT-based data.
- The current database indicates that the value ranking of the Ao/So magnitude ratio for different source types remains in the same order as a function of source depth. Since this result is for a single radiation direction, it is to be expected that obtaining this ratio for other radiation directions will supplement the WT-based data with possibly sufficient information to uniquely classify the AE source type even with changing source depth. This expectation is based upon the fact that different source types have different AE-energy radiation patterns. Thus a series of WT-based magnitude ratios from a total number, n, of different radiation angles (e.g., $(Ao/So)_1$, $(Ao/So)_2$, …, $(Ao/So)_n$) could form an input vector to an artificial intelligence (AI) software program that would determine the AE source type. The AI program could be initially trained using a FEM-generated database.

B. Source Identification–Small Coupon Specimens

- The inherent multiple edge reflections present in small coupon specimens complicate the use of WT coefficients for source identification. Since the current small coupon FEM database does not include (except for one case) the important parameter (relative to edge reflection effects) of changes in specimen side-to-side position of the source, the current database did not allow a full examination of these complications.

Acknowledgement

This work was partially supported by NASA Langley. We wish to express our gratitude to Prof. Takemoto, who released the source code of the wavelet transform software his group had developed and made AGU-Vallen Wavelet available. We also thank Dr. Y. Mizutani and Mr. Jochen Vallen for making the program into a highly usable form. Their contributions have significantly advanced the field of AE.

References

D. J. Buttle and C. B. Scruby, "Characterization of Fatigue of Aluminum Alloys by Acoustic Emission, Part 1-Identification of Source Mechanism", Journal of Acoustic Emission, **9**, No. 4, 1990a, 243-254.

D. J. Buttle and C. B. Scruby, "Characterization of Fatigue of Aluminum Alloys by Acoustic Emission, Part II – Discrimination Between Primary and Secondary Emissions", Journal of Acoustic Emission, **9**, No. 4, 1990b, 255-269.

Dawei Guo, Ajit K. Mal and Marvin A. Hamstad, “AE Wavefield Calculations in a Plate”, in *Progress in Acoustic Emission IX*, Acoustic Emission Working Group and Acoustic Emission Group, 1998, pp. IV-19 to IV-29.

M. A. Hamstad, A. O'Gallagher and J. Gary, "Modeling of Buried Acoustic Emission Monopole and Dipole Sources With a Finite Element Technique", Journal of Acoustic Emission, **17**, No. 3-4, 1999, 97-110.

R. L. Mehan and J.V. Mullin, “Analysis of Composite Failure Mechanisms Using Acoustic Emissions”, Journal of Composite Materials, **5**, April 1971, 266-269.

W. H. Prosser, M. A. Hamstad, J. Gary and A. O'Gallagher, "Reflections of AE Waves in Finite Plates: Finite Element Modeling and Experimental Measurements", Journal of Acoustic Emission, **17**, No. 1-2, 1999, 37-47.

H. Suzuki, T. Kinjo, Y. Hayashi, M. Takemoto and K. Ono, “Wavelet Transform of Acoustic Emission Signals”, Journal of Acoustic Emission, **14**, No. 2, 1996, 69-84.

M. Takemoto, H. Nishino and K. Ono, "Wavelet Transform - Applications to AE Signal Analysis", Acoustic Emission - Beyond the Millennium, Elsevier (2000), pp. 35-56.

Vallen-Systeme GmbH, Münich, Germany, http://www.vallen.de/wavelet/index.html, 2001.

R. Weaver and Y. H. Pao, “Axisymmetrical Waves Excited by a Point Source in a Plate”, Journal of Applied Mechanics, **49**, 1982a, 821-836.

R. Weaver and Y. H. Pao, “Spectra of Transient Waves in Elastic Plates”, Journal of the Acoustical Society of America, **72**, 1982b, 1933-1941.

H. Yamada, Y. Mizutani, H. Nishino, M. Takemoto and K. Ono, "Lamb Wave Source Location of Impact on Anisotropic Plates", Journal of Acoustic Emission, **18**, (2000, December), 51-60.

A WAVELET TRANSFORM APPLIED TO ACOUSTIC EMISSION SIGNALS: PART 2: SOURCE LOCATION[#]

M. A. HAMSTAD[+], A. O'GALLAGHER and J. GARY

National Institute of Standards and Technology, Materials Reliability Division (853),
Boulder, CO 80305-3328;
[+]Also Department of Engineering, University of Denver, Denver, CO 80208.

Abstract

In Part 2, the same finite-element-generated database of acoustic emission (AE) signals was used, as in Part 1: Source Identification, to examine the application of a wavelet transform (WT) to improve the accuracy of AE source location. These signals represented the top surface out-of-plane displacement versus time from buried dipole sources in aluminum plates 4.7 mm thick. The method utilizes a WT result to select AE signal-arrival times for a single group velocity from energetic modes. The cases of both the large plate without edge reflections and the small plate (coupon) with multiple edge reflections were examined. The arrival time of a specific frequency of an energetic fundamental mode of the far-field signals was determined from the WT. Using these arrival times at three propagation distances, a group velocity was determined for comparison with the appropriate group velocity based on dispersion curves. Both filtered narrow-band (100 to 300 kHz) and wideband (40 kHz high-pass) signals were examined. In addition, in the large-plate case, experimental sensor/preamplifier electronic noise was added to the AE signals to examine the effect of noise on the determination of accurate arrival times as a function of signal-to-noise (S/N) ratios. Results for the large plate indicate that very accurate arrival times can be determined that correspond to a particular group velocity. In the coupon case, the results indicate significant distortions in the arrival times due to the multiple edge reflections. The perturbation due to the presence of electronic noise was relatively small for the case of the wideband signals in the large plate until signal-to-noise ratios reached levels where an AE hit would likely not be recorded.

1. Introduction

One of the important aspects of acoustic emission (AE) technology is the ability to use the arrival times of the signals (from a single event) at three or more sensors to calculate the location of the source in the test object. Often the two-dimensional location in a plate is determined. The standard technique combines the measured arrival times with an appropriate single propagation velocity to calculate the source location. In most AE applications, the arrival times of the signals are obtained from the time that the signals first penetrate a fixed voltage threshold. As has been documented (Hamstad, 1986; Gorman, 1990; Hamstad and Downs, 1995), this approach leads to location errors. In particular, the arrival times at the different sensors often are determined from different unknown velocities. This situation is a direct result of both the AE source characteristics (for example the source strength) and effects of the propagation of dispersive Lamb waves along with geometry-based attenuation. The net result is that source location may be calculated on the basis of inconsistent data. Specifically, the arrival times are not all obtained at the same

[#] Contribution of the U.S. National Institute of Standards and Technology; not subject to copyright in the US.

velocity, and the velocity used in the location calculation is not the correct one for each sensor hit.

Some previous research has demonstrated an approach to decrease the location errors (Ziola and Gorman, 1992). In this approach, cross-correlation techniques were used to determine the arrival times for a particular mode (typically the flexural mode) and frequency. The AE signals analyzed were obtained from sensors responding to out-of-plane surface displacements. These arrival times were combined with a corresponding theoretical group velocity to calculate a more accurate source location. The resulting improvement in location accuracy was demonstrated by out-of-plane pencil-lead breaks on the surface of a plate test specimen. This validation approach is potentially incomplete. First, out-of-plane lead breaks create relatively large flexural mode (anti-symmetric) components of the AE signals as compared to real AE sources, which can be dominated by in-plane dipoles with smaller flexural-mode signals. Second, the surface lead breaks do not account for the substantial differences in the dominate mode in AE signals as a function of the depth of a real AE source through the plate thickness, as was shown in Part 1 (Hamstad et al., 2002).

In the research reported here, we examine the use of a wavelet transform (WT) to accurately obtain arrival times at known group velocities from realistic modeled AE signals. We utilized AGU-Vallen Wavelet program for obtaining WTs as in Part 1 (Hamstad et al., 2002). The AGU group first used WT for determining the group velocity dispersion of the Lamb waves (Cho et al., 1996; Hayashi et al., 1999) and for AE source location on anisotropic CFRP plates (Yamada et al., 2000; Takemoto et al., 2000). Yamada et al. (2000) determined the group velocity of flexual Lamb waves (generated by pencil-lead breaks or ball drops) from the maxima of WT coefficients of a certain frequency. A few other research works used a WT for AE source location (Yamada et al., 2000; Takemoto et al., 2000; Kwon and Joo, 2000, Jeong and Jang, 2000). The validation approach used in these experimental studies is incomplete due to the reliance on monopole sources from out-of-plane pencil-lead breaks or ball drops on the plate surface. In this work, we obtained the AE signals in plate samples by finite-element modeling (FEM), and the sources of these signals include realistic dipoles as well as the important variable of source depth. The modeled signals also have the advantage that the exact three-dimensional source location is known. Thus, WT-based signal-arrival times at different propagation distances can be quantitatively evaluated for their correspondence to a single group velocity.

2. Signal Database and Wavelet Transform

An AE signal database of plate top surface out-of-plane displacement as a function of time at three propagation distances was used. The AE signal database, specimen geometry and the relevant WT information were described in detail in Part 1 (Hamstad et al., 2002) of this two-part paper. Hence, we have not repeated that description here.

3. WT−Based Source Location (Large Plates)

The extraction of arrival times from the WTs of AE signals was successively examined by several approaches. The first approach was based on the results of a WT of the simulated wideband AE signals that had been filtered with a 40 kHz high-pass filter. In this case, the information extracted from the WT result consisted of data pairs of arrival time and frequency based upon absolute peaks of the WT's magnitude (WT coefficient). When sets of such data pairs were compared for three different propagation distances from a given AE source, it was deter-

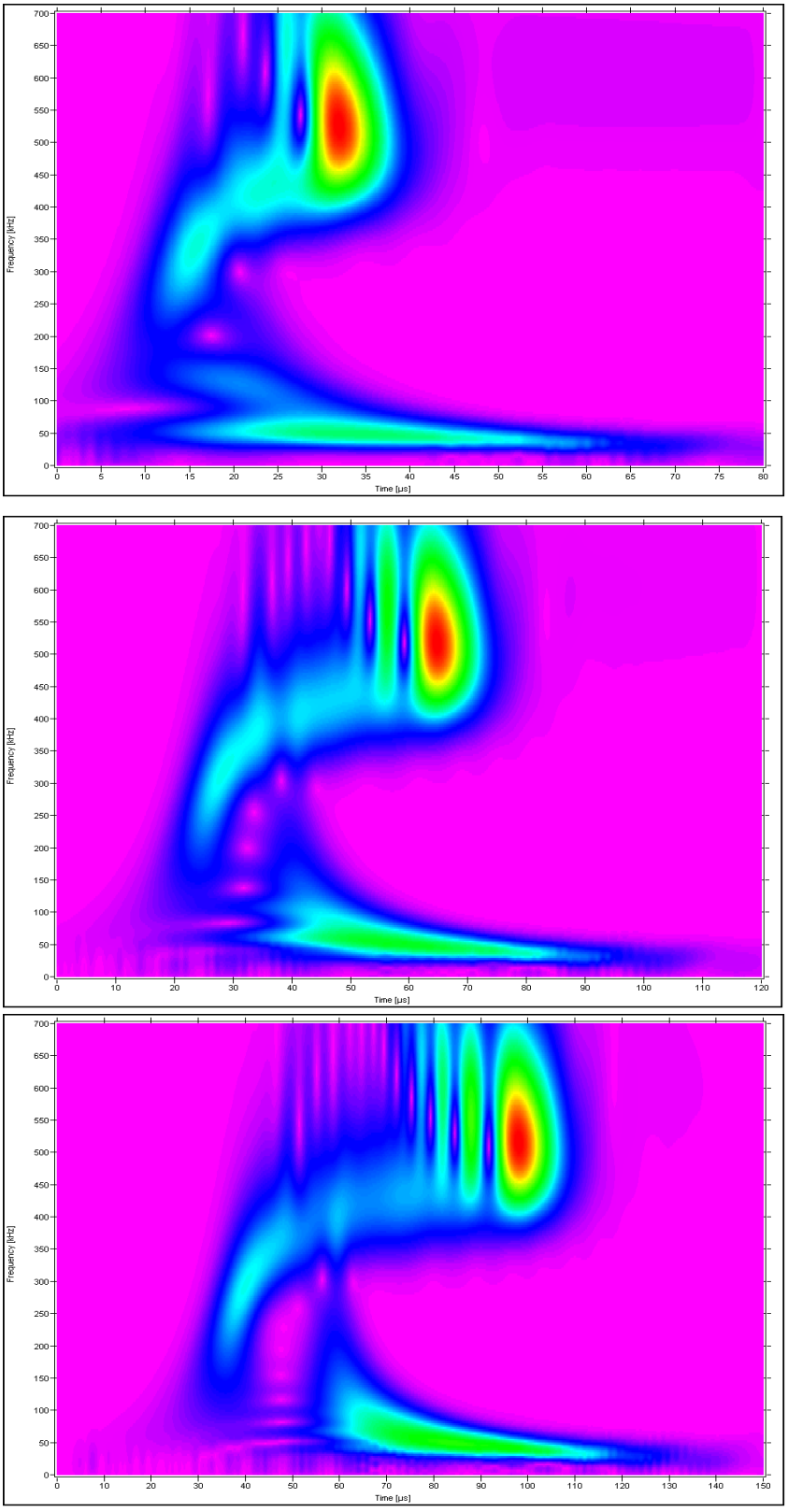

Fig. 1 WT plots used to determine AE signal arrival times from the peak WT magnitudes of the So mode at 522 kHz. The AE source was an in-plane dipole at a depth of 2.037 mm with propagation distances of (a) 60 mm, (b) 120 mm, and (c) 180 mm. AE signals filtered with 40 kHz high pass filter prior to WT. Frequency (0 to 1 MHz) versus time (a: 0 to 80 µs, b: 0 to 120 µs, and c: 0 to 150 µs from top to bottom).

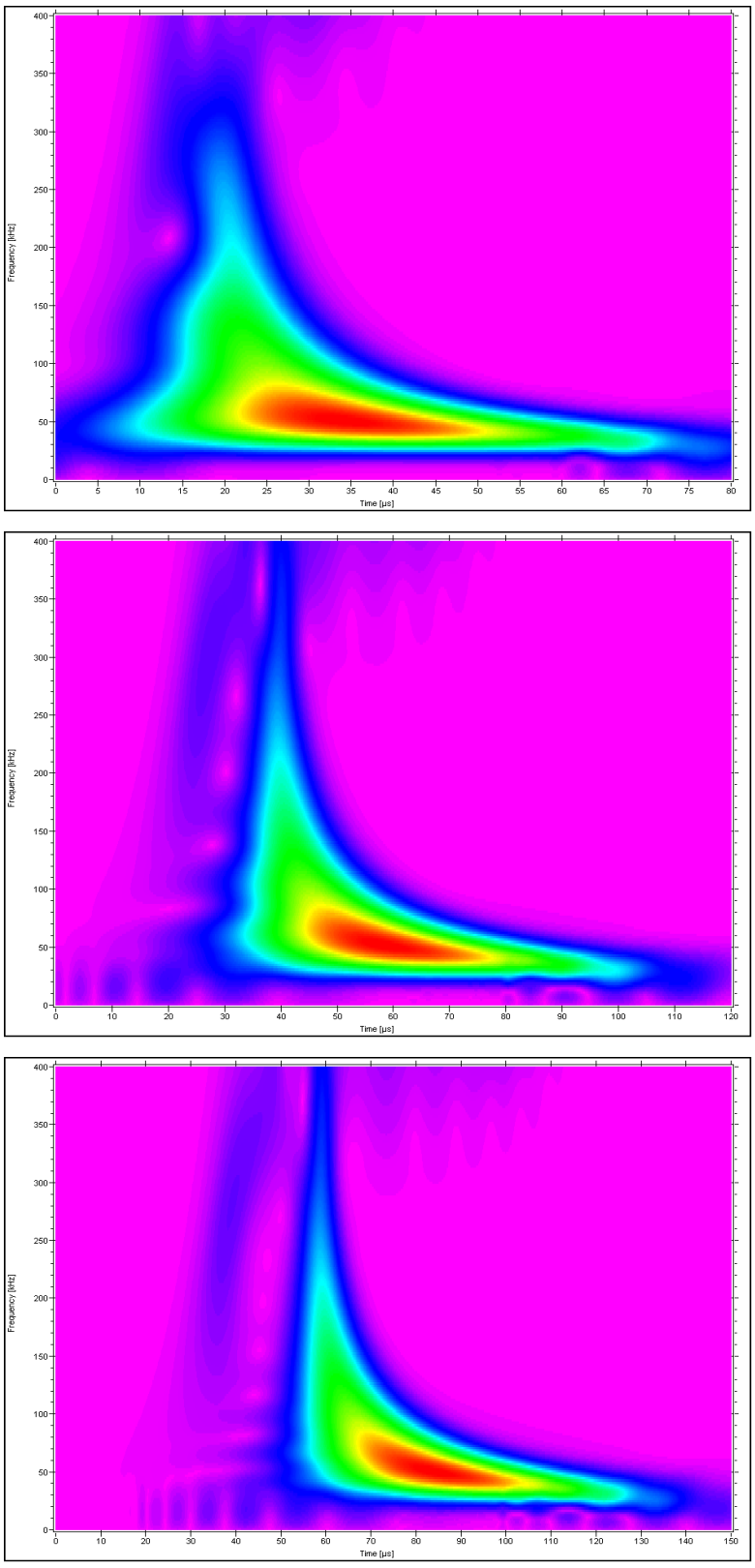

Fig. 2 WT plots used to determine AE signal arrival times from the peak WT magnitudes the Ao mode at 66 kHz. The AE source was an in-plane dipole at a depth of 0.783 mm. The propagation distances and filter were the same as for Fig. 1(a), (b), and (c). Frequency (0 to 400 kHz) versus time (same scales as Fig. 1; 1 MHz vs. a: 80 µs, b: 120 µs, and c: 150 µs top to bottom).

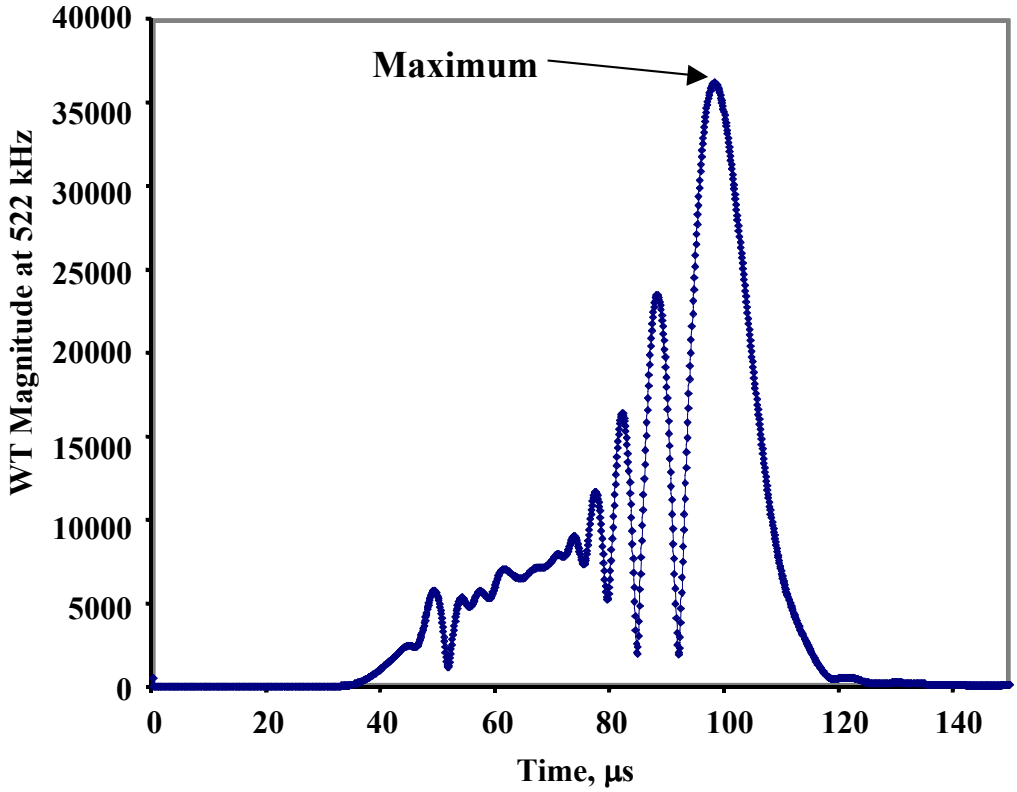

Fig. 3 Example of the WT magnitude versus time for the So mode at 522 kHz from the WT result shown in Fig. 1(c). Plot illustrates the determination of the arrival time of the peak magnitude near the selected group velocity of the mode.

mined that there were differences in the frequency values of the maximum magnitude as a function of propagation distance. Since determining arrival times at different frequencies and thus different group velocities at each sensor would complicate the process of source location, it seemed best to examine alternative approaches so that the simplest use of WT data to extract arrival times could be developed.

The second approach that was examined was based upon choosing a single frequency for a particular fundamental Lamb symmetric (So) or anti-symmetric (Ao) mode. Based upon the modal region of the WT that had a large magnitude, a single frequency was chosen in the same fashion as the source-identification approach in Part 1 (Hamstad et al., 2002). Then, using this frequency, the arrival time of the maximum magnitude of the WT at that frequency (and associated mode) was determined, as was done by Yamada et al. (2000). It was found that choosing the parameters of the WT to enhance the resolution and smoothness (as discussed in Part 1: Hamstad et al., 2002) of the WT result was important to facilitate the determination of the maximum at the selected frequency and mode. To initially examine this approach in more depth, two different in-plane dipole source cases were chosen. In one case the source depth was chosen such that the maximum magnitudes of the WT were in the lower-frequency regime of the fundamental anti-symmetric mode. In the other source-depth case, the maximum magnitudes of the WT were in the higher-frequency regime of the fundamental symmetrical mode. Table 1 shows the arrival times obtained at the indicated frequencies and modes (Ao, 66 kHz and So, 522 kHz) for the three available propagation distances (60, 120, 180 mm). In contrast to Part 1, a higher frequency was used for Ao to be more certain that the arrival times would not be altered by the 40 kHz high-pass filter. Figures 1 and 2 show the high-resolution WT results, which were used in the two cases. The WT-parameters used were Wavelet size (WS) = 600 samples, Maximum Fre-

Table 1. Arrival times (μs) of the peak WT magnitude for in-plane dipole source signals filtered with a 40 kHz high-pass filter in the large plate.

So mode at 522 kHz						Ao mode at 66 kHz				
Source	Distance, mm			Velocity, mm/μs		Distance, mm			Velocity, mm/μs	
depth, mm	60	120	180	Slope	Theoretical	60	120	180	Slope	Theoretical
2.037	31.9	64.6	98	1.82	1.78	-	-	-	-	-
0.783	-	-	-	-	-	29.1	51.9	75.1	2.61	2.61

quency (MF) = 700 kHz, Frequency Resolution (FR) = 3 kHz for the signal dominated by the So mode and WS = 600 samples, MF = 400 kHz, FR = 2 kHz for the signal dominated by the Ao mode. The sources were at depths of 2.037 mm (Fig. 1 for the dominant symmetric mode) and 0.783 mm (Fig. 2 for the dominant anti-symmetric mode). Figure 3 shows a plot of the WT magnitude as a function of time at a single frequency of 522 kHz for the 180 mm distance case of Fig. 1. The time of arrival of the maximum WT magnitude for the selected mode and frequency was obtained from the available spreadsheet that gives the WT magnitude (WT coefficient) as a function of time and frequency. The time resolution of the spreadsheet was 0.1 μs, which is the same resolution as the re-sampled simulated AE signal. Since the exact locations of the source and sensors are known, the information in Table 1 can be plotted to form distance-versus-time plots. The slopes of these plots provide group velocities as well as coefficients of determination (R^2) for the straight line fits. Table 1 shows these slope-based group velocities as well as the group velocity (for the mode and frequency) available from the relevant theoretical dispersion curves. Figure 4 shows an example of one of the plots (for the Fig. 1 case, 2.037 mm source depth) of distance versus arrival time along with the equation that describes the straight-line fit. The plot (not shown) of the other case (0.783 mm depth) gave a similar straight-line fit. The excellent straight-line fits imply that the arrival times correspond very closely to a single group velocity that is quite near the theoretical group velocity.

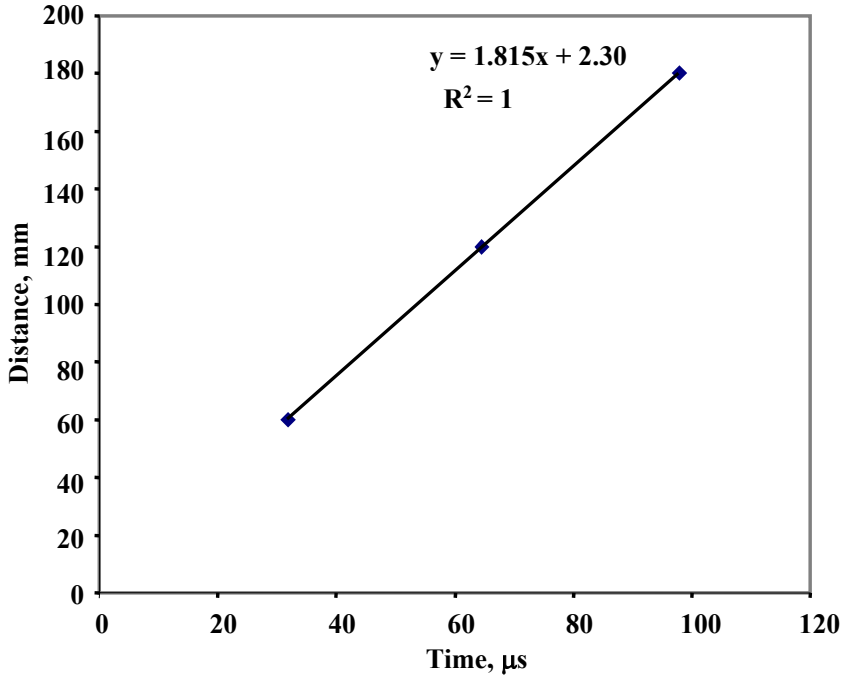

Fig. 4. Plot of propagation distances versus arrival time of peak magnitude of the So mode at 522 kHz for the WTs in Fig. 1. Equation of straight-line fit with slope of 1.815 mm/μs representing the slope-based group velocity. $R^2 = 1$, correlation coefficient.

Table 2. Arrival times (μs) of the peak WT magnitude for in-plane dipole source signals filtered with a 100 to 300 kHz bandpass in the large plate.

Source	Distance, mm			Velocity, mm/μs		Distance, mm			Velocity, mm/μs	
depth, mm	60	120	180	Slope	Theoretical	60	120	180	Slope	Theoretical
2.037	15.9	28.2	40.5	4.88	4.88	-	-	-	-	-
0.783	-	-	-	-	-	25.2	45.7	65.7	2.96	3.00

It is worthwhile to point out that the straight-line fit has an intercept that does not pass through the source origin (even with an excellent fit, $R^2 = 1$, of the data to a straight line). The reason for this behavior is likely due to the fact that the wave propagation needs to progress over some number of plate thicknesses in order to fully develop the Lamb modes at their propagation velocity. We also note that the group velocities determined from the WTs of the finite element data did not always correspond exactly to those determined from the theoretical group velocity (dispersion) curves. For example, when the arrival times used to calculate the indicated velocity in Table 1 of Part 1 (Hamstad et al., 2002) were used along with the propagation distances to obtain a plot of distance versus time the slope-based group velocity was 2.45 mm/μs. This value is 1.2 % faster than the dispersion curve velocity of 2.42 mm/μs for the Ao mode at 50 kHz. As will be seen later in the description of a proposed source location procedure, we suggest the group velocities determined from WT results might be expected to provide more accurate results. But the correctness of this assumption will need to be determined through additional research.

A third approach was also examined. This approach was really just a deviation of the second one. In this case the modification was to filter the FEM-based signals with a 100 to 300 kHz bandpass filter before calculating the WTs. This frequency range was chosen since it has often been used in experimental AE applications. Figure 5 (Fig. 1 case) and Figure 6 (Fig. 2 case) show the resulting high-resolution WT results for the same two sources. These WT results were calculated for the filtered signals, which are also shown in Figs. 5 and 6. The WT-parameters used were WS = 600 samples, FR = 2 kHz, and MF = 400 kHz. In this case the maximum magnitudes of the WTs are in a different frequency range. Table 2 shows the selected frequencies and modes (Ao, 134 kHz and So, 262 kHz) for each case as well as the arrival times determined from the WTs; also shown are the group velocities from the plots of distance versus time and the group velocities from the dispersive group-velocity curves at the selected frequencies and modes. The slope-based group velocities shown in Table 2, again, were quite close to those obtained from dispersion curves. As before, the plots of distance versus arrival time had excellent fits but again did not pass through the origin, presumably due to the need to propagate several plate thicknesses to develop the Lamb modes and their group velocities. Thus, in this range of bandpass frequency, the arrival times correspond very closely to a single group velocity very near the theoretical velocity.

4. Proposed Method of WT-Based Source Location for Experimental Data (Large Plate)

The results above indicate that the approach of using a fixed frequency of an energetic mode to determine an arrival time at the maximum magnitude of a WT (Yamada et al., 2000) could result in accurate arrival times that are associated with a particular wave mode and corresponding group velocity. But, since the calculated group velocities from the finite-element data did not always correspond exactly to the dispersion-curve values, it may be useful to account for this aspect. By providing for this aspect, it may be possible to obtain the best possible experimental location accuracy with a WT-based technique. The approach we suggest would use the group

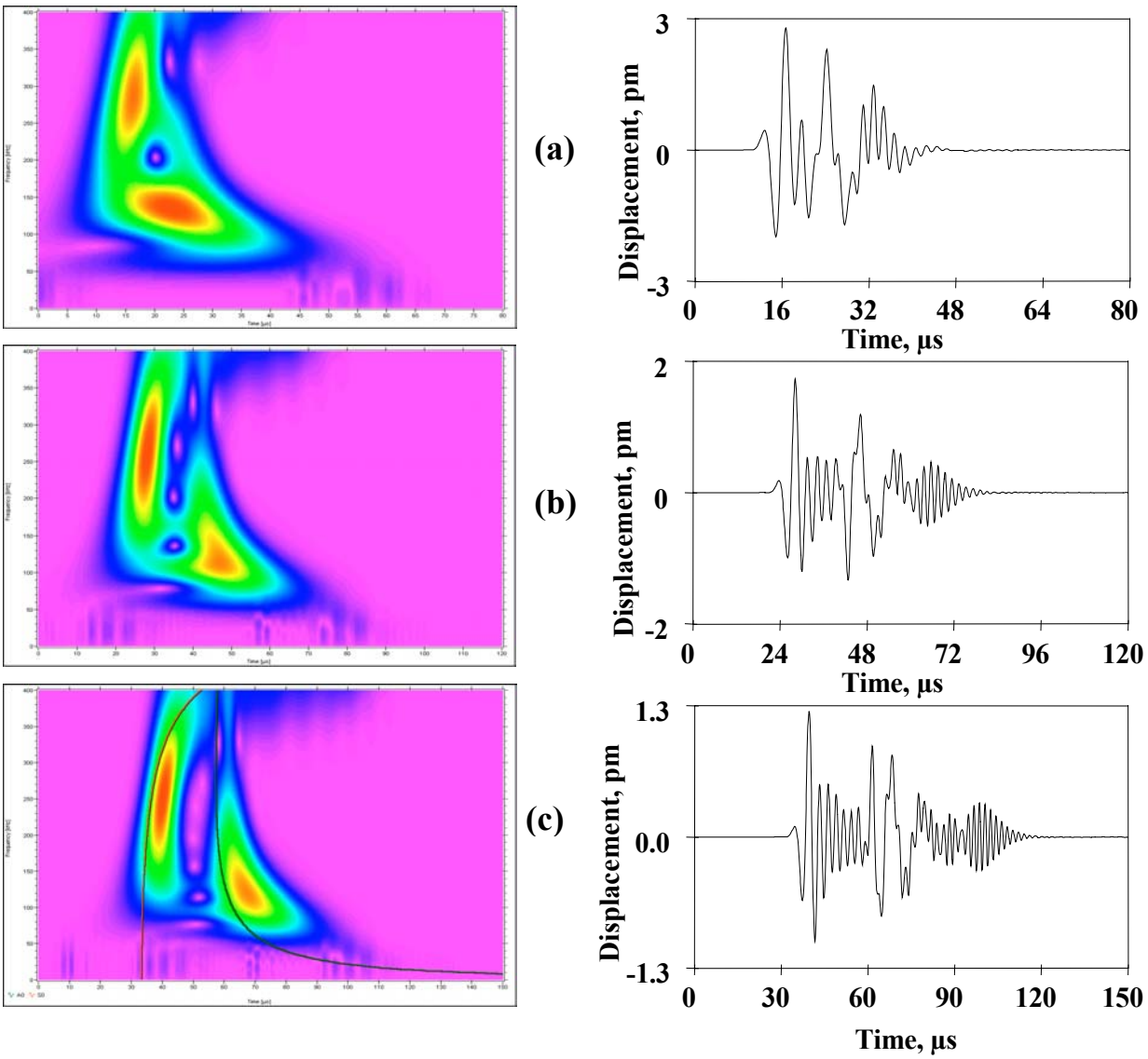

Fig. 5 WT results (frequency 0 to 400 kHz versus time (0 to 80, 0 to 120, and 0 to 150 µs)) for the same cases shown in Fig. 1 but with a 100 to 300 kHz bandpass filter prior to calculating the WT. Fig. 5(c) also shows superimposed Ao and So group-velocity-based dispersion curves after conversion to arrival times based on the propagation distance of 180 mm. Also shown are the corresponding filtered AE signals.

velocity from the dispersion-based curves as an initial group-velocity estimate. Possibly a better group-velocity value could be determined as described below by pre-experiments. The pre-experiment approach would replace that illustrated in Fig. 4 since the propagation distances used to construct that figure are available only for the FEM data. We point out that the "calibrated" group velocity extracted from Fig. 4 could be viewed as compensating for small differences in group velocity (compared to dispersion-based values) induced by the WT algorithm. Presumably these algorithm-induced differences would be a part of each WT calculation with a particular algorithm. Also, the pre-experiments would be necessary when accurate group velocities cannot be calculated.

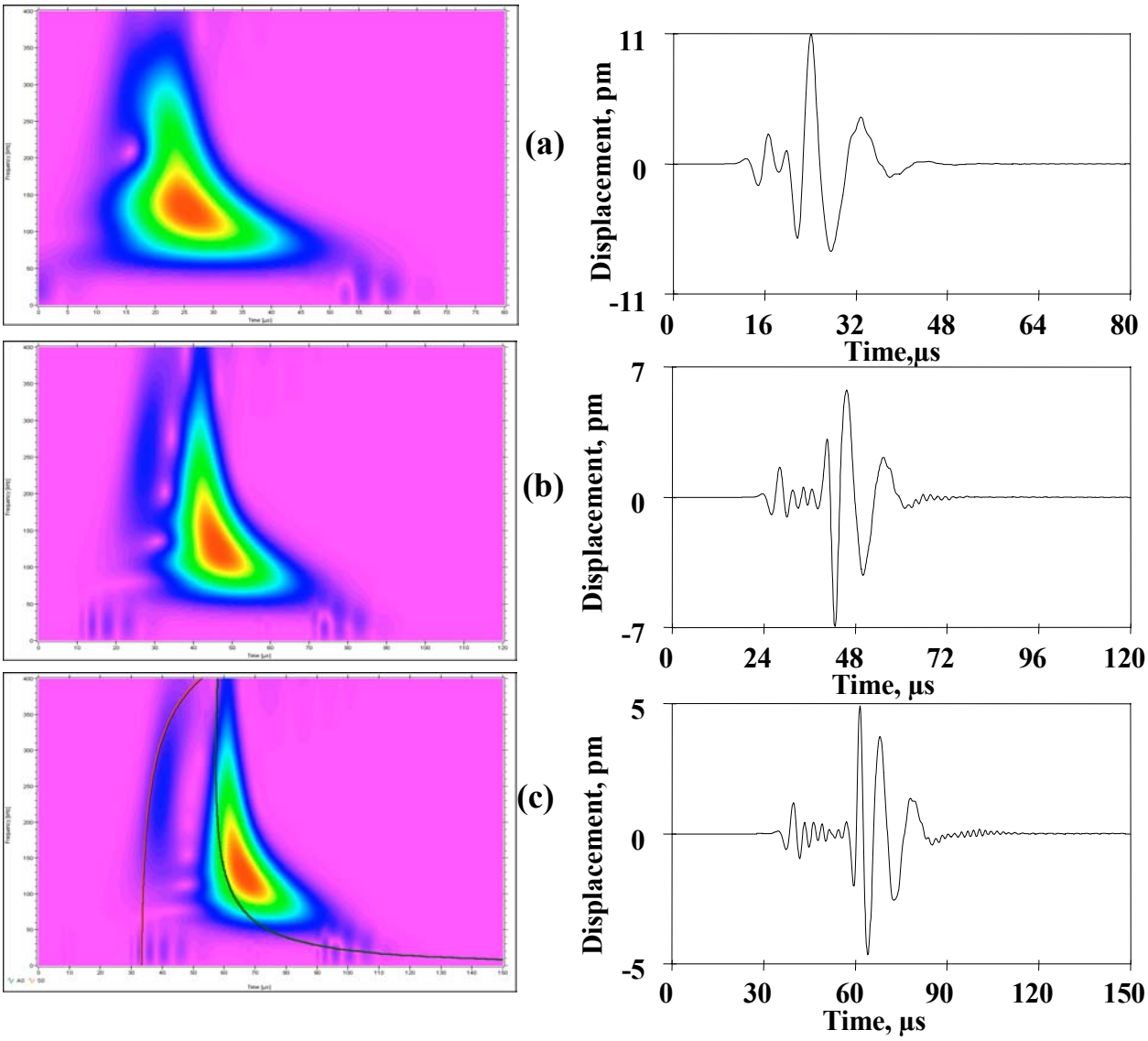

Fig. 6 WT results (same scales as Fig. 5) for the same cases shown in Fig. 2 but with a 100 to 300 kHz bandpass filter prior to calculating the WT. Fig. 6(c) shows the superimposed Ao and So group-velocity-based dispersion curves after conversion to arrival times based on the propagation distance of 180 mm. Also shown are the corresponding filtered AE signals.

5. Comments Relative to the Location Approach for Real AE Signals

With actual AE data, in particular narrow-band data, the preliminary task of selecting the wave mode to associate with the WT maximum magnitude region may require some pre-experiments. The purpose of conducting pre-experiments with pencil lead breaks and the real sensors would be to identify the mode(s) associated with the peak magnitude frequency range(s) of the WT and to determine corresponding WT-based group velocities. A large plate of the same thickness and material could be used for these pre-experiments. Good control of the position and force direction of the lead break is necessary. But in principle, an in-plane pencil break on the plate edge close to the top or bottom surfaces would allow identification of the dominant-energy WT frequencies for the anti-symmetric modes (typically for thin plates this will be the fundamental anti-symmetric mode). And an in-plane lead break located almost exactly at the mid-

plane could allow (with careful filtering) the determination of the dominant frequencies of the peak-magnitude region of the WT for the symmetric modes (typically for thin plates this is expected to be the fundamental symmetric mode). These frequencies and modes could then be used with dispersion-based group-velocity curves to provide the initial estimates of the group velocities to be used to calculate the source location. In addition WTs from sensors at several accurately known distances from these experimental sources could be used to obtain "calibrated" group velocities (as referred to above).

In contrast to the source-identification task with a subset of WT data, the dependence of the WT results on source depth does not cause significant problems in determining source location. It is necessary only to add a step in the calculation of source location that determines which mode is dominant in an AE signal by calculating appropriate Ao/So ratios as described in Part 1 (Hamstad et al., 2002). Based on the ratio determined, the most energetic mode and associated frequency can be used to extract the WT-based arrival times. Also, the correct group velocity for the dominant mode and frequency for each AE signal can be selected for the calculation of the source location.

6. Effects of Electronic Noise

In experimental cases, the AE signal is a combination of signal (from the AE source) and noise (from the electronics). Thus, to be useful, the above method of WT-based source location must retain its determination of accurate arrival times for a single group velocity in the case of experimental signals that combine signal and noise. To examine this issue we added electronic noise to the calculated FEM signals and studied the WT-based determination of arrival times. The study was carried out as a function of the signal-to-noise (S/N) ratio.

The noise signals were taken from two different wideband sensor/preamplifier combinations. These experimental signals were obtained with the wideband sensors coupled only to air. In addition, the sensors were protected from any possible laboratory airborne signals. Prior to being added to the FEM calculated signals, the noise signals were filtered with a six-pole digital Butterworth filter from 40 kHz to 1.2 MHz. As Fig. 7 shows, the typical spectra of the noise signals were considerably different from each other. In one case the electronic noise increases significantly with decreasing frequency. In the other case, the electronic noise amplitude is distributed more uniformly with frequency, with a peak region near the middle of the frequency range. By using noise signals with these two different spectrums, we attempted to broaden the results of the study.

Also to broaden the results of the study, two distinctly different FEM calculated signals were selected. In one case, a higher-frequency region of the fundamental symmetric mode dominated the AE signal energy. In the second case, a lower-frequency region of the fundamental anti-symmetric mode dominated the AE signal energy. The source for both signals was an in-plane dipole located at 180 mm from the sensor. In the case of the dominant symmetric mode the source was at a depth of 2.35 mm (mid-plane). The dominant anti-symmetric-mode source was at a depth of 0.47 mm below the top surface of the large plate.

In order to quantitatively characterize the S/N ratio, the peak amplitudes of the noise and the calculated AE signals (40 kHz high-pass) were determined over the 150 μs portion of each signal used in the WTs. Then the noise signals were multiplied by appropriate factors to obtain the desired range of S/N ratios, based on the peak amplitudes.

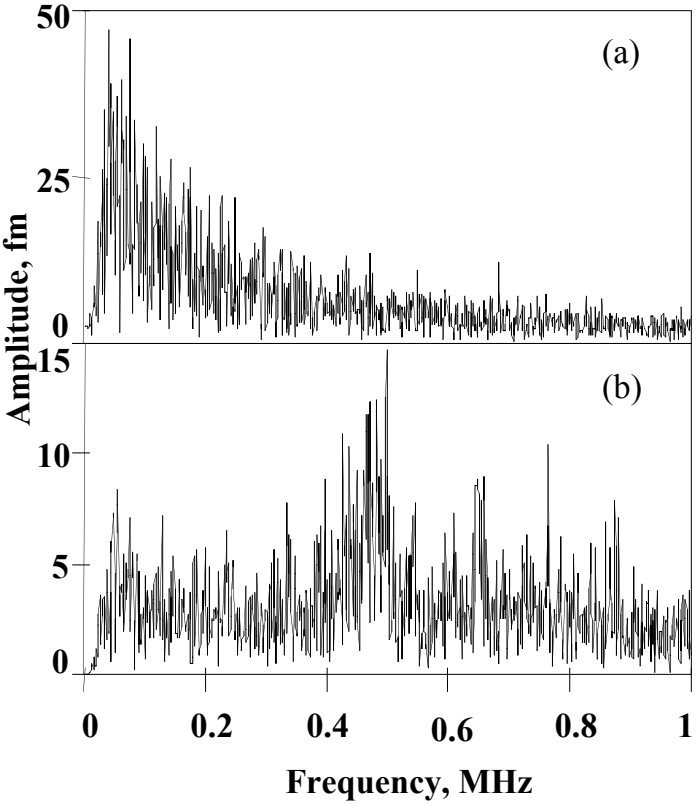

Fig. 7 Typical frequency spectra for the two experimental noise signals calculated from an 819.2 μs signal length. Low-frequency emphasis (a) and distributed frequencies (b).

Figure 8 shows the WTs of the two calculated AE signals ((a) and (b) without added noise) and the two noise signals ((c) and (d)). These WTs were calculated with the following high-resolution parameters (WS = 600, FR = 3 kHz [0-600 kHz case] and 2 kHz [0-400 kHz case]). Following the approach used earlier in this paper, the arrival times of the peak magnitudes of the WTs were determined at 522 kHz (AE signals dominated by the symmetric mode) and at 66 kHz (AE signals dominated by the anti-symmetric mode). Table 3 shows the determined arrival times at 522 kHz for the two different noise types at the selected S/N ratios. Table 4 shows the arrival times at 66 kHz for the two noise cases. No arrival times are shown in the tables when the peak magnitude of the WTs was not obvious. In all cases the WTs were calculated with the high-resolution parameters used to produce Fig. 8.

Table 3. Arrival times (μs) determined from the peak WT magnitude at 522 kHz for the original AE signal dominated by a higher-frequency region of the fundamental symmetric mode.

S/N ratio	Noise dominated by low frequencies	Noise with distributed frequencies
no noise	97.9	97.9
10:1	97.9	97.9
5:1	97.9	97.9
2:1	97.9	97.9
1:1	97.9	97.8
1:2	97.9	87.8
1:5	101.8	117.2
1:10	101.8	–
Noise signal	33.1, 101.5	115.9, 15.5

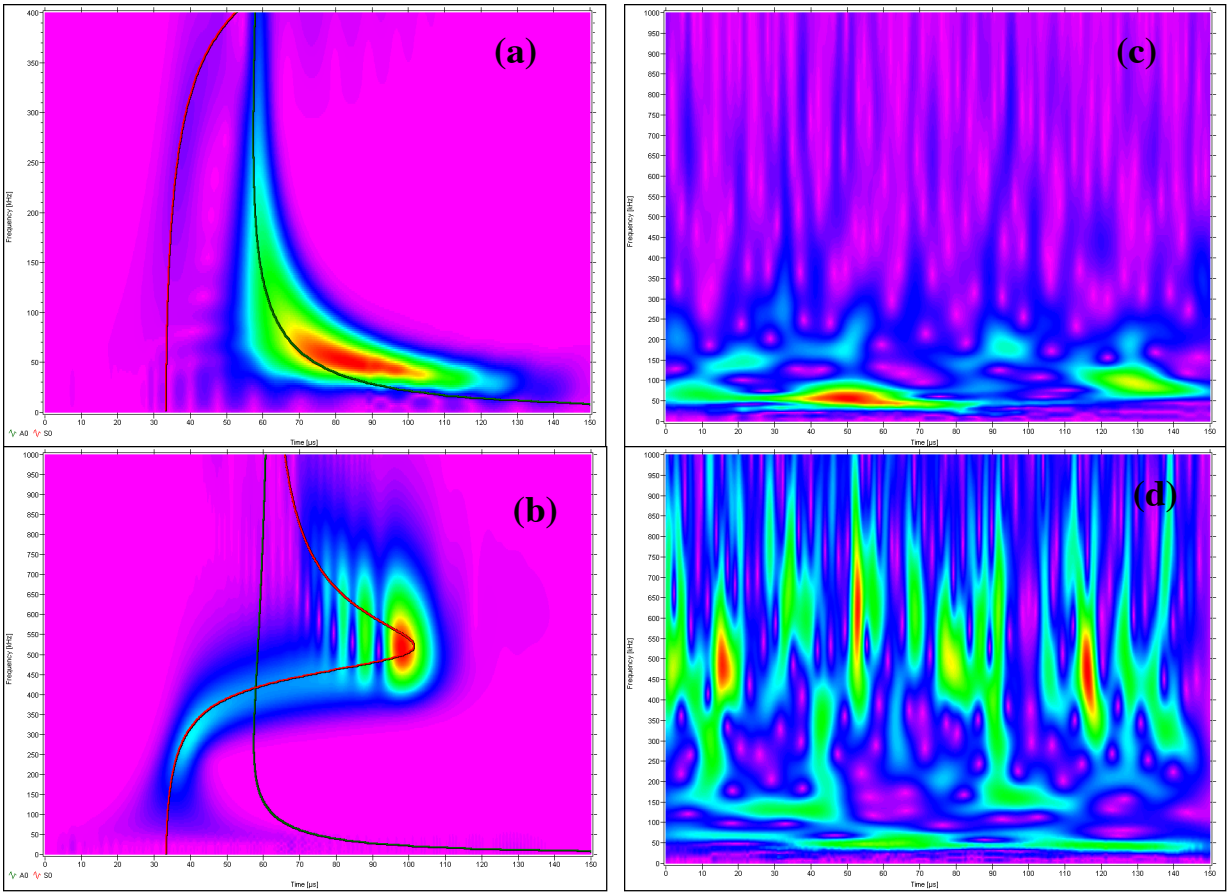

Fig. 8 WTs of the calculated AE signals and the experimental electronic noise for 150 μs length signals: (a) for AE signal at 180 mm propagation distance with dominant fundamental anti-symmetric mode; (b) for AE signal at 180 mm propagation distance with dominant fundamental symmetric mode; (c) for electronic noise with low-frequency emphasis; and (d) for electronic noise with distributed-frequency emphasis.

Table 4. Arrival times (μs) determined from the peak WT magnitude at 66 kHz for the original AE signal dominated by a lower frequency region of the fundamental antisymmetric mode.

S/N ratio	Noise dominated by low frequencies	Noise with distributed frequencies
no noise	75.1	75.1
10:1	75.6	75.2
5:1	76.1	75.3
2:1	77.1	75.6
1:1	80.3	76.1
1:2	47.7	76.2
1:5	–	74.6
1:10	–	26.7
Noise signal	49.2	66.6, 24.4

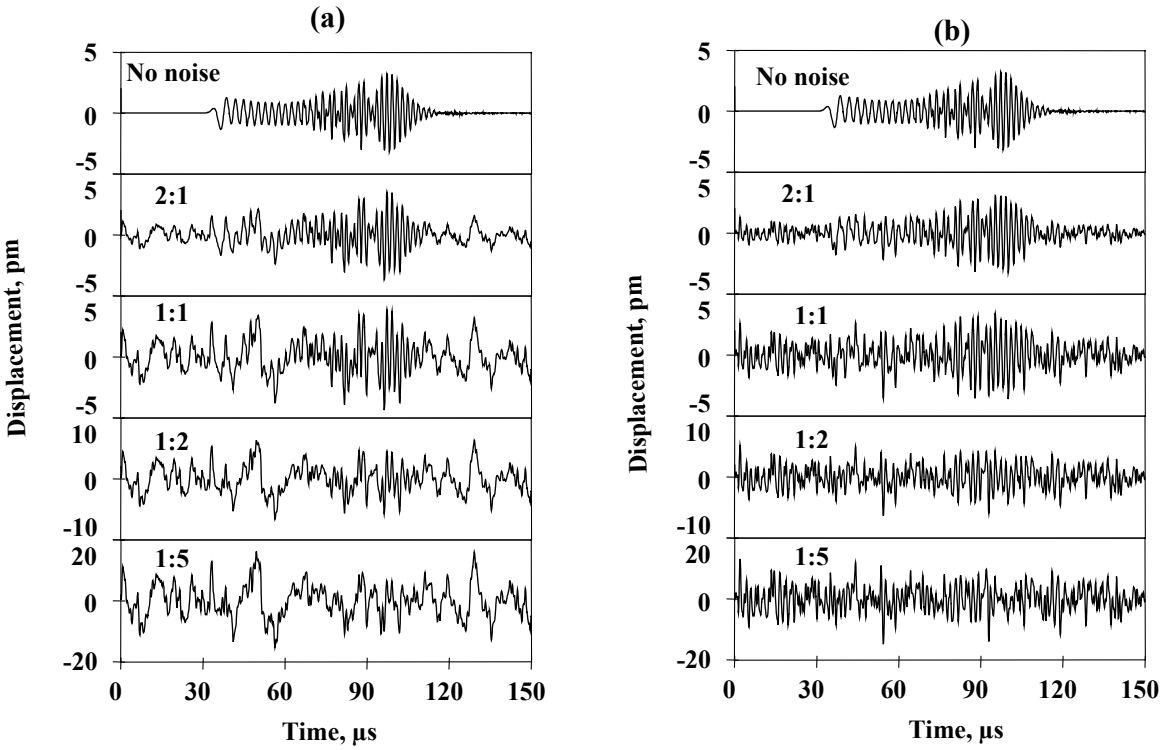

Fig. 9 Waveforms of signal-plus-noise at the indicated S/N ratios for the AE signal at 180 mm propagation distance dominated by the fundamental symmetric mode: (a) noise with low-frequency emphasis; (b) noise with distributed-frequency emphasis.

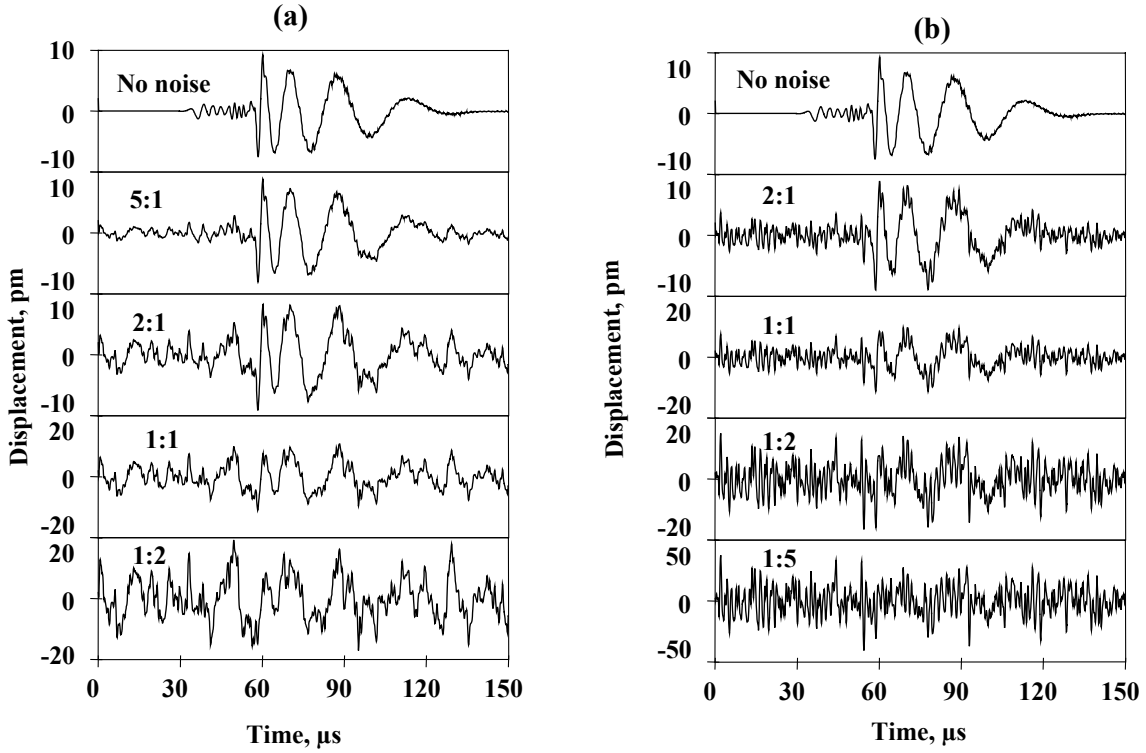

Fig. 10 Same types of waveforms as Fig. 9 for the AE signal at 180 mm propagation distance dominated by the fundamental anti-symmetric mode.

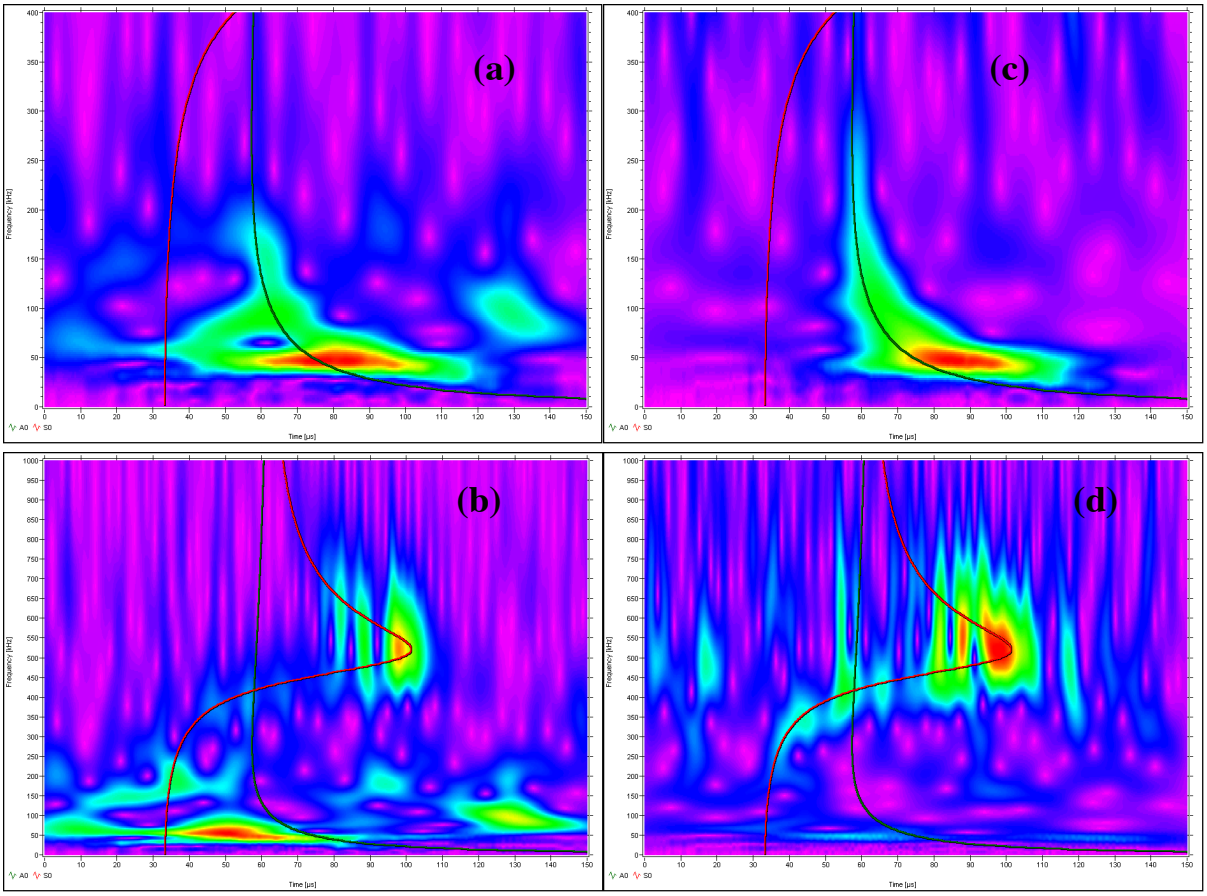

Fig. 11 WTs of waveforms of signal plus noise. Signals at 180 mm from the in-plane dipole source. The noise in (a) and (b) was dominated by low frequencies and in (c) and (d) by distributed frequencies. The signal in (a) and (c) was dominated by the fundamental anti-symmetric mode from the source at a depth of 0.47 mm. In (b) and (d) the signal was dominated by the fundamental symmetric mode from the source at a depth of 2.35 mm. The signal-to-noise ratio in each case was 1:1.

To provide a clearer understanding of the results in Tables 3 and 4, Fig. 9 shows selected waveforms of signal-plus-noise for the two noise cases when the original AE signal was dominated by a higher-frequency region of the symmetric mode. Figure 10 shows the same type of selected results when a lower-frequency region of the anti-symmetric mode dominated the original AE signal. Examination of the above figures and tables reveals several key aspects about the effects of electronic noise on the WT-determination of arrival times from a particular mode and frequency. First, when the S/N ratio becomes too small, the arrival time of the WT magnitude peak typically moves toward the WT peak magnitude of the noise signal (at the selected frequency). Second, even with a relatively poor S/N ratio of 1:1 as shown in Figs. 9 and 10, the WT-based arrival time is still reasonably accurate. As Figs. 9 and 10 show for these cases, it is becoming difficult to extract by eye the AE signal. And clearly, a threshold-based technique would lead to inaccurate arrival times (or no hit detected) not associated with a known group velocity. The worst result at this 1:1 ratio is the case of the signal dominated by the low-frequency anti-symmetric mode and the noise dominated by low frequencies. Since WTs result in better time resolution at higher frequencies, it is possible that the slightly poorer accuracy at 66 kHz is due to the characteristics of the WT. More likely, the result is due to the frequency peaks of the original AE signal and the noise being in the same frequency range. This conclusion

is based on the observation (see Tables 3 and 4) that errors in the arrival times appear at higher S/N ratios when the noise and original signals have peaks in the same frequency region.

The reason why reasonably accurate arrival times can be extracted from the WT results at S/N ratios of 1:1 or less seems to be due to the fact that the WT spreads out the noise over the bandpass frequency range while preserving the spread of the noise in time. Determinations of arrival times by penetration of a fixed threshold have the noise spread out only in time. Thus, such approaches typically cannot even detect an AE hit at S/N ratios as low as 1:1. Figure 11 demonstrates at a S/N ratio of 1:1 that the WT of the AE signal plus noise is dominated in all four cases by the same WT region that dominated when only the AE signal was present (compare Fig. 11 with Figs. 8(a) and 8(b)). In Fig. 11 the four cases of AE signal plus noise are: (a) low-frequency noise and low-frequency AE signal; (b) low-frequency noise and high-frequency AE signal; (c) distributed noise and low-frequency AE signal; (d) distributed noise and high-frequency AE signal.

We did not investigate the narrow-band S/N ratio case, since we did not have available the digital displacement calibration of a typical 150 kHz resonant commercial AE sensor. Thus, we could not properly alter the calculated sensor signal for the AE source to correspond to the sensor resonance. We expect that the above WT-based method of detection of arrival times would not be as robust at low S/N ratios, since both the AE signal and the noise would be concentrated in the same relatively narrow frequency range.

An additional positive of the WT-based method, in the case of wideband waveform-based AE measurement systems, may be that fewer AE events would have only one useable hit. If the measurement system were configured so that all the waveforms from a group of sensors were recorded when one sensor was hit (i.e. a signal above the threshold), then WT-based processing could extract relevant arrival times from the sensor channels where threshold-penetration hits would not occur. Thus, signal arrival times corresponding to a single group velocity could be extracted from the channels where the AE signal had attenuated into the background electronic noise. And potentially a source location could be calculated for an event where it could not be calculated with a threshold-based AE system.

7. WT for Source Location in Samples with Nearby Edges

When the lateral size of the test specimen is decreased so that nearby edges are present, the AE signals and their WTs become much more complicated. This result was illustrated in Part 1 (Hamstad et al., 2002) in Figs. 16 and 17. Since the distribution of WT-illustrated signal energy in these figures does not clearly follow the shapes of the superimposed fundamental Lamb-mode curves from the dispersion relations, the use of the approaches developed for source location in the large plate might be expected to experience difficulties for the coupon specimen. Further, since the distortion of the WT results is due to edge reflections, moving the source from side-to-side across the 25.4 mm width of the coupon specimen will change the reflections and WTs as was illustrated in Fig. 18 of Part 1 (Hamstad et al., 2002). The current coupon database, except for the case illustrated in Fig. 18 of Part 1 (Hamstad et al., 2002), does not include the side-to-side variation of the source position.

In spite of the limited database (side-to-side source position), we examined for the coupon specimen the application of the techniques applied to the large-plate signals. The results of this examination in the coupon (using 40 kHz high-pass signals) for the same source cases used in the

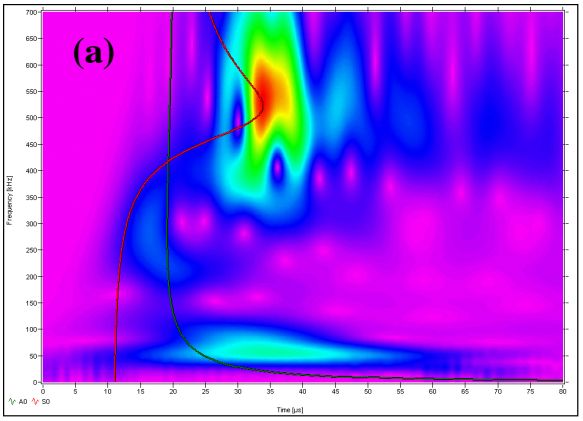

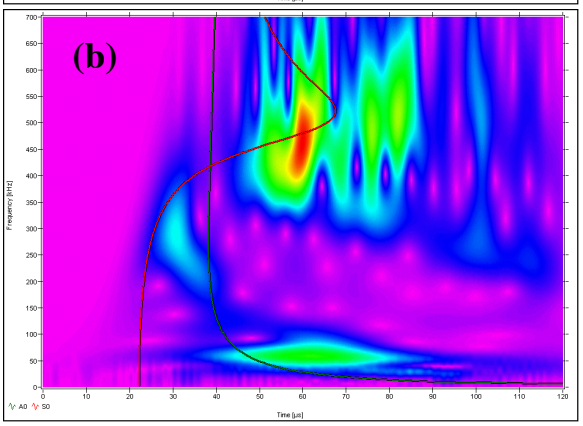

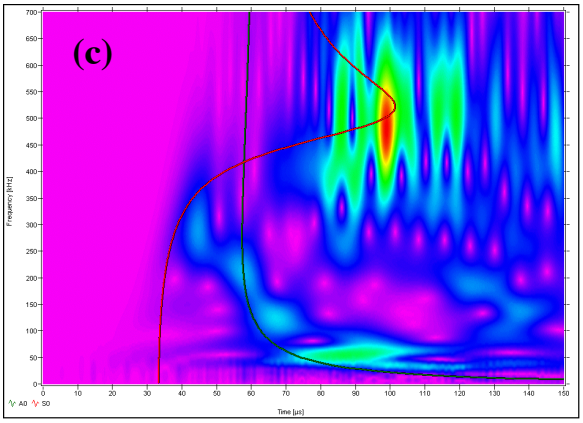

Fig. 12 WT plots used to determine AE signal arrival times from the peak magnitudes of the So mode at 522 kHz for the coupon specimen. The AE source was an in-plane dipole at a depth of 2.037 mm with propagation distances of (a) 60 mm, (b) 120 mm, and (c) 180 mm. AE signals filtered with 40 kHz high-pass filter prior to WT. Frequency (0 to 700 kHz) vs. time (0 to 80, 0 to 120, 0 to 180 μs from top to bottom). Superimposed group velocity curves of fundamental modes.

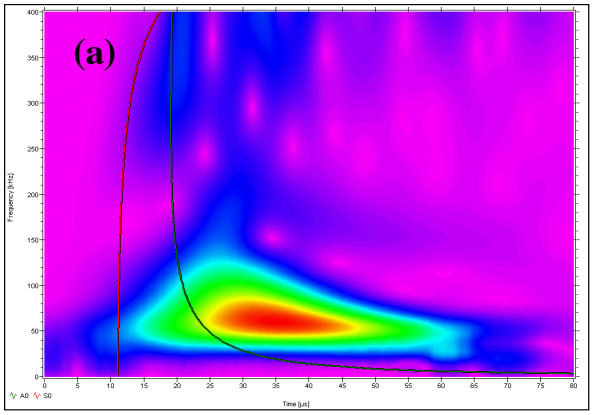

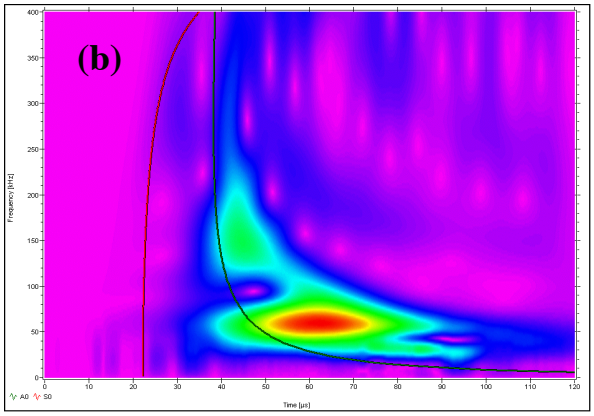

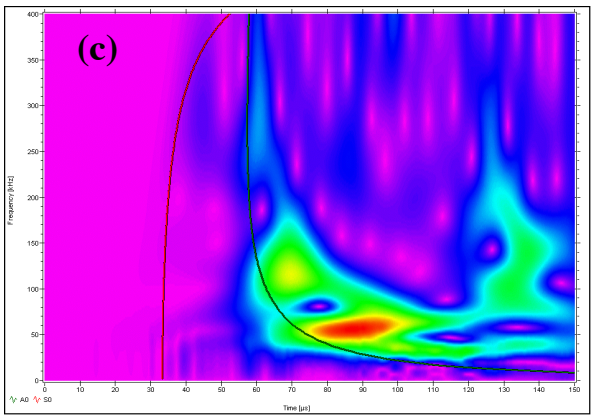

Fig. 13 WT plots used to determine AE signal arrival times from the peak magnitudes of the Ao mode at 66 kHz for the coupon specimen. The AE source was an in-plane dipole at a depth of 0.783 mm. The propagation distances and filter were the same as for Fig. 12 (a), (b), and (c). Frequency (0 to 400 kHz) versus time (same scales as Fig. 12, top to bottom).

Table 5. Arrival times (μs) of the peak WT magnitude for in-plane dipole source signals filtered with a 40 kHz high-pass filter in the coupon specimen.

	So mode at 522 kHz					Ao mode at 66 kHz				
Source	Distance, mm			Velocity, mm/μs		Distance, mm			Velocity, mm/μs	
depth, mm	60	120	180	Slope	Theoretical	60	120	180	Slope	Theoretical
2.037	33.8	60	99	1.82	1.78	-	-	-	-	-
0.783	-	-	-	-	-	33.8	61.9	91.2	2.09	2.62

large plate (those that lead to Figs. 1 and 2 and Table 1) are shown in Figs. 12 and 13 and Table 5 for the coupon. For the WT calculations the WS = 600 samples was used for both modes; and the FR and MF values used were 2 kHz and 400 kHz for the Ao mode and 3 kHz and 700 kHz for the So mode. The maximum WT magnitude arrival times were selected while ignoring reflections from the ends of the coupon specimen. Figure 12 shows the WTs for the coupon for the in-plane dipole at a depth of 2.037 mm. Figure 13 shows the coupon WTs for a depth of 0.783 mm. The source position for the results shown in Figs. 12 and 13, as well as Table 5, was located half-way across the coupon (12.7 mm form the side). Table 5 indicates the results were mixed. For the 2.037 mm depth and the So mode at 522 kHz, the slope-determined velocity of 1.82 mm/μs was the same as the large plate velocity of 1.82 mm/μs, but in the plot of distance versus arrival time the data did not fit the straight-line slope very well. For the 0.783 mm depth and the Ao mode at 66 kHz the slope-determined velocity in the coupon was 2.09 mm/μs (again data with a poor fit) which was 20 % lower than the value of 2.61 mm/μs in the large plate.

Table 6. Arrival times (μs) of the peak WT magnitude for in-plane dipole source at 2.35 mm depth and different distances from the coupon side. So mode at 522 kHz.

	Distance, mm			Velocity, mm/μs	
Case	60	120	180	Slope	Theoretical
Coupon, 3.31 mm	32.4	65.1	87.8	2.13	1.78
Coupon, 6.13 mm	36.4	77.7	103.8	1.75	1.78
Coupon, 12.7 mm	33.9	60	98.7	1.82	1.78
Large plate	31.9	64.6	97.9	1.82	1.78

To study the effect of side-to-side variation of the source position, we applied the same approach (522 kHz WT-peak arrival time) to the cases for the in-plane dipole at the mid-plane depth of 2.35 mm. Table 6 (same WT-parameters as for Table 5) shows the results (40 kHz high-pass data) for the coupon with the source at three different distances (12.7, 6.13, and 3.31 mm) from the coupon side compared to the equivalent large plate case. For convenience, the propagation distances are reported as 60, 120, 180 mm, but in determining the slope-based group velocities the actual straight-line distances from the source to the sensors were used. Table 6 clearly shows significant differences in the slope-determined group velocity (of the fundamental symmetric mode at a frequency of 522 kHz) as a function of transverse source position. Compared to the velocity determined from the large-plate signals (for the same case) the group velocity changes range from 0.6 % to 17 %. It is also clear from Table 6 that the arrival times at the different sensors vary over a considerable range compared to the large plate values, which were not influenced by the side-edge reflections. Figure 14 compares the differences in the WT magnitude versus time at 522 kHz for the large plate compared to the coupon specimen with the source at 3.31 mm from the coupon side. This figure is for the sensor located at the nominal propagation distance of 180 mm. The alteration of the peak arrival time in the coupon specimen is clearly visible along with the generally significantly larger magnitudes of the WT in that case.

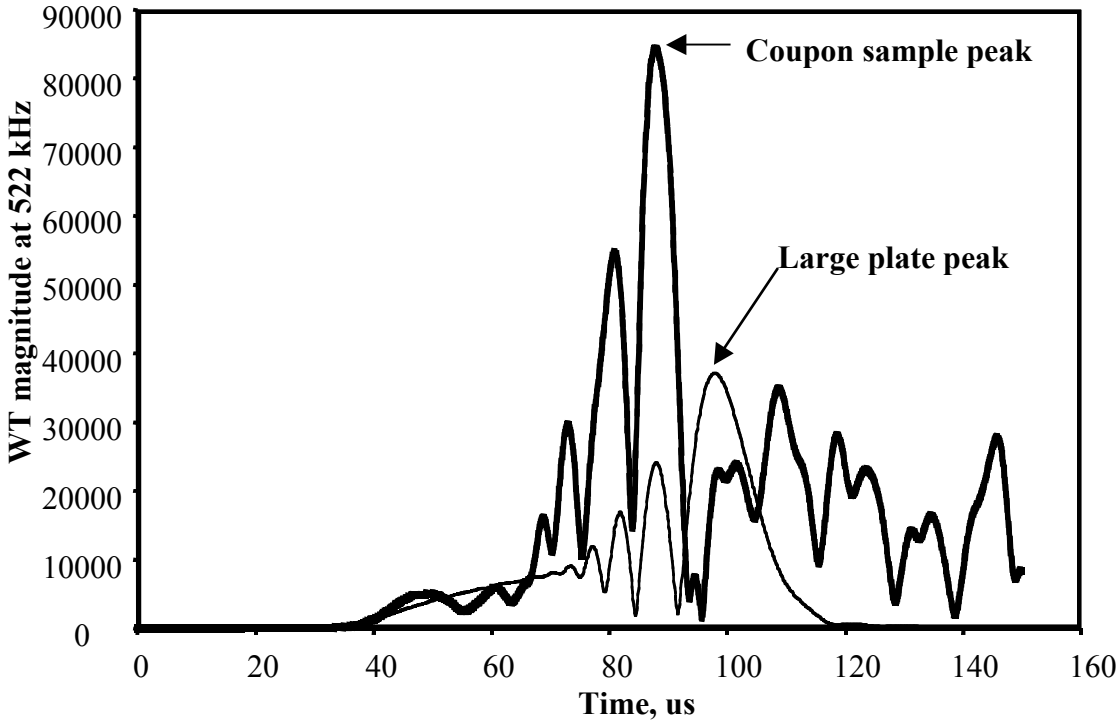

Fig. 14 WT magnitude at 522 kHz versus time for a large plate and coupon specimen. In both cases the source was an in-plane dipole at a depth of 2.35 mm and a propagation distance of 180 mm. The coupon source was located at 3.31 mm from the coupon side.

We conclude that significant and variable errors can be present in the arrival times for the coupon specimens when they are determined by the WT approach examined here. The errors in coupon-determined group velocities could be overcome by appropriate pencil lead-break data from a large-plate specimen of the same material and plate thickness as the coupon specimen, but arrival-time errors would remain. These errors would result in poor accuracy for source location calculations.

The effect of the side-to-side transverse source position was also examined using signals that had been filtered from 100 to 300 kHz. The WTs were calculated with high-resolution parameters (WS = 600 samples, MF = 400 kHz and FR = 2 kHz) for the in-plane dipole at a depth of 2.35 mm. Table 7 compares the three small coupon cases with the equivalent large-specimen results and the dispersion-curves-based group velocity at 262 kHz. As was the case above, the arrival time at maximum WT magnitude was selected by ignoring a magnitude maximum caused by reflections from the coupon-specimen's ends. The propagation distance versus the arrival times was plotted to determine the group velocity for each case of transverse source position. Compared to the large-plate data, the straight-line fits to the data for distance versus time were poor. The best fit was for the symmetrical center-line source position. But, even in that case, the group velocity was reduced by 13 % compared to the large-plate velocity. The group velocity determined when the source was located 6.13 mm from the coupon edge was very close to the result determined for the large plate. However, this was happenstance as the straight-line fit was very poor. Figure 15 shows the excellent fit and equation for the large plate as well as the significant error and typical scatter (relative to a straight line) of the three small-coupon cases. Thus, again, we conclude that side-edge reflections distort the determination of accurate arrival times. Obviously, inaccurate arrival times would lead to significant errors in source location.

Table 7. Arrival times (μs) of the peak WT magnitude for in-plane dipole sources at 2.35 mm depth and different distances from the coupon side. Signals were filtered from 100-300 kHz and the So mode at 262 kHz was used.

	Distance, mm			Velocity, mm/μs	
Case	60	120	180	Slope	Theoretical
Coupon, 3.31 mm	15.3	34.8	46.8	3.74	4.89
Coupon, 6.13 mm	26.4	44.5	47	4.89	4.89
Coupon, 12.7 mm	19.4	34.4	47.6	4.25	4.89
Large plate	15.8	28.3	40.5	4.86	4.89

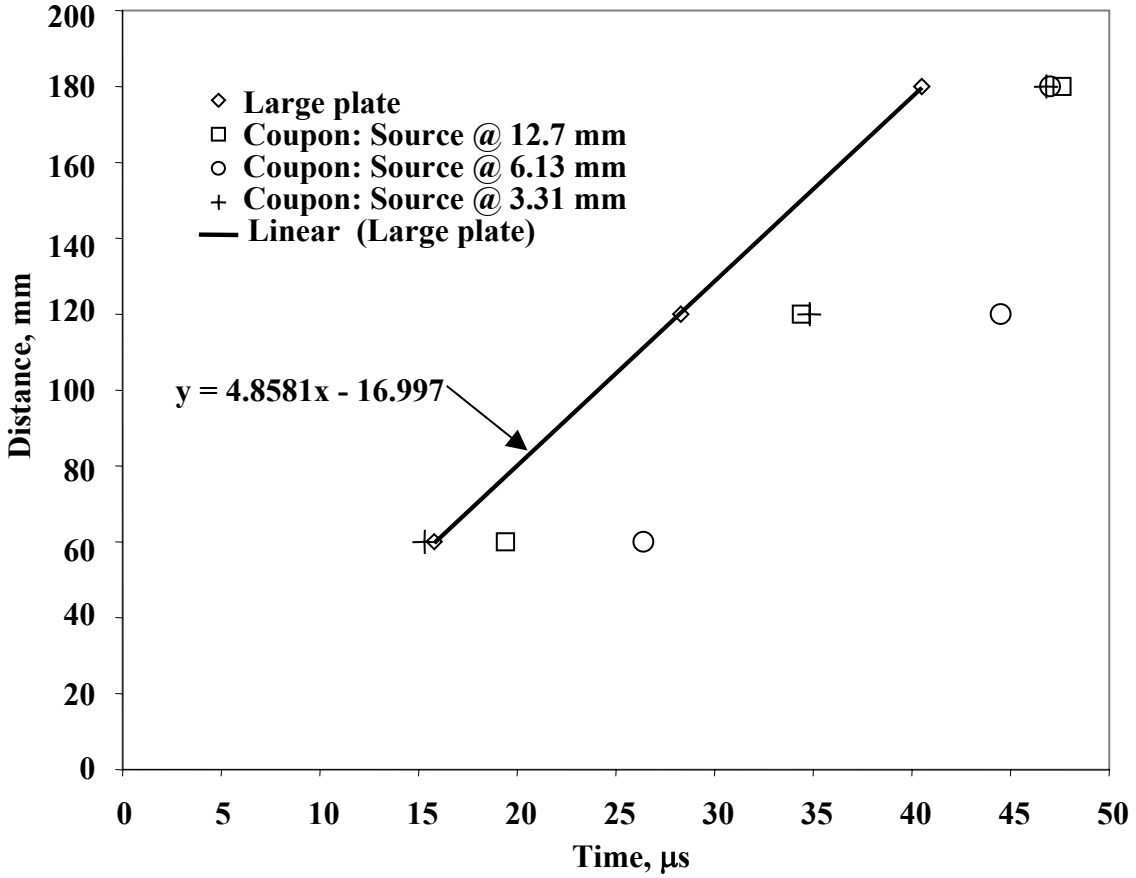

Fig. 15 Excellent fit of distance versus arrival time from WT peak magnitude at 262 kHz for large plate as compared to scatter and consequent lack of straight line fit for coupon specimen cases with variation in source distance from specimen side. AE signals were filtered from 100 to 300 kHz prior to the WT. Source was an in-plane dipole at a depth of 2.35 mm below the plate surface.

8. Conclusions

A. Source Location–Large Plates

- Excellent straight-line correlations of propagation distance versus the WT-based arrival times of the fundamental modes at fixed frequencies indicate that source location in large plates

can be significantly enhanced by use of WT results compared to that possible with fixed thresholds and an assumed constant group velocity.

- Since the amount of energy in a particular mode depends on the source depth, it will be necessary to first select the mode with the dominant energy in each AE signal. Then WT-based arrival times of the maximum WT magnitude of the experimental AE signals can be obtained from that mode at a selected frequency.
- In experimental situations, carefully applied pencil-lead breaks can be used to determine the key frequency to use for each dominant mode. Then only the WT-based arrival times and peak magnitudes at these frequencies need to be extracted. The source location can then be directly calculated from the arrival times for the mode with the dominant peak magnitude. The group velocity for the calculation could be taken from dispersion curves for the selected mode and frequency or from a WT-based group velocity obtained during pre-experiments with careful pencil lead breaks.
- The technique for extraction of WT-based arrival times corresponding to a single group velocity was found to be applicable for both wideband and narrow-band signals.
- In the wideband case, the extraction of single-velocity arrival times was found to be robust in the presence of electronic noise even for signal-to-noise ratios as low as 1:1.

B. Source Location–Small Coupon Specimens

- The inherent multiple side-edge reflections present in small-coupon specimens complicate the use of the WT for the purpose of obtaining accurate source locations.

Acknowledgement

This work was partially supported by NASA Langley.

References

H. Cho, S. Ogawa and M. Takemoto, "Non-contact Laser Ultrasonics for Detecting Subsurface Lateral Defects", NDT and E International, **29**-5, 1996, 301-306.
Hayashi et al., 1999

M. R. Gorman, "Plate Wave Acoustic Emission", Journal of the Acoustic Society of America, **90** (1), 1990, 358-364.

M. A. Hamstad, "On Determination of Arrival Times for Acoustic Emission Source Location in Composites", *Proceedings AECM-2*, Society of the Plastics Industry, New York, New York, 1986, pp. 202-208.

M. A. Hamstad, A. O'Gallagher and J. Gary, "Examination of the Application of a Wavelet Transform to Acoustic Emission Signals: Part 1. Source Identification", Journal of Acoustic Emission, **20**, 2002, 39-61. (preceding paper)

M. A. Hamstad and K. S. Downs, "On Characterization and Location of Acoustic Emission Sources in Real Size Composite Structures – A Waveform Study", Journal of Acoustic Emission, **13**, No. 1–2, 1995, 31-41.

Yasuhisa Hayashi, Shingo Ogawa, Hideo Cho and Mikio Takemoto, “Non-contact estimation of thickness and elastic properties of metallic foils by the wavelet transform of laser-generated Lamb waves”, NDT and E International, **32**-1, 1999, 21-27.

Hyunjo Jeong and Young-Su Jang, “Fracture Source Location in Thin Plates Using the Wavelet Transform of Dispersive Waves”, IEEE Transactions on Ultrasonics, Ferroelectrics and Frequency Control, **47**-3, 2000, 612-619.

O.Y. Kwon and Y.C. Joo, “Source Location in Plates by Using Wavelet Transform of AE Signals”, Journal of Acoustic Emission, **18**, 2000, S212-221.

M. Takemoto, H. Nishino and K. Ono, "Wavelet Transform - Applications to AE Signal Analysis", *Acoustic Emission - Beyond the Millennium*, Elsevier, 2000, pp. 35-56.

H. Yamada, Y. Mizutani, H. Nishino, M. Takemoto and K. Ono, "Lamb Wave Source Location of Impact on Anisotropic Plates", Journal of Acoustic Emission, **18**, 2000, 51-60.

Steven M. Ziola and Michael R. Gorman, “Acoustic Emission Source Location in Thin Plates Using Crosscorrelation”, *Proceedings AECM-4*, The American Society for Nondestructive Testing Inc., Columbus, OH, 1992, pp. 411-417.